

TECHNICAL UNIVERSITY OF CRETE

---

# Numerical Simulation and forecasting of wind waves

---

March 4, 2019

PANAGIOTA KERAMEA  
Advisor: A.Delis  
Comittee:M.Mathioudakis, N.Kampanis

# Contents

<b>1</b>	<b>Introduction</b>	<b>1</b>
<b>2</b>	<b>Description of the Delft3D model</b>	<b>5</b>
2.1	Physical processes . . . . .	8
2.2	The Delft3D - FLOW model . . . . .	8
2.3	The Delft3D - WAVE model . . . . .	16
2.3.1	Wave height and period . . . . .	17
2.3.2	Spectral description of wind waves . . . . .	18
2.3.3	Propagation in an inhomogeneous medium . . . . .	23
2.3.4	Action and Energy balance equation . . . . .	25
2.4	Boundary conditions . . . . .	29
2.4.1	Vertical boundary conditions . . . . .	29
2.4.2	Open boundary conditions . . . . .	30
2.4.3	Closed boundary conditions . . . . .	34
2.5	Numerical aspects . . . . .	34
<b>3</b>	<b>Data Analysis</b>	<b>37</b>
3.1	About Copernicus . . . . .	37
3.2	Procedure of CMEMS . . . . .	38
3.3	R program and connection with open boundary conditions . . . . .	39
3.4	Procedure of Delft Dashboard . . . . .	39
<b>4</b>	<b>Test case and model setup</b>	<b>43</b>
4.1	Swan Model set-up . . . . .	44
4.2	Results and Discussion . . . . .	46
4.2.1	Water Level . . . . .	46
4.2.2	Currents . . . . .	52
4.2.3	Observation Points . . . . .	62
4.2.4	Swan Wave Model . . . . .	67
4.2.5	Conclusion and Recommendations . . . . .	69
<b>5</b>	<b>References</b>	<b>70</b>

## **Abstract**

In this study we describe the wind wave fields. The general aims of the work are the estimation of statistical wave parameters and the assessment of interannual and seasonal wave parameter variability. Wave parameters will be calculated by means of the SWAN wave model on a relatively fine rectangular grid. Initial conditions (wind speed and direction) for a historical period will be derived from the reanalysis NCEP/NCAR..

## Περίληψη

Στην παρούσα διπλωματική εργασία θα γίνει προσομοίωση, πρόβλεψη και ανάλυση των ανεμογενών κυματισμών. Στόχος αυτής της διπλωματικής εργασίας είναι η εκτίμηση των κυματικών παραμέτρων (ύψος, περίοδος κυματισμών) και της εποχικής και ετήσιας μεταβλητότητας τους. Οι κυματικές παράμετροι θα υπολογισθούν με τη βοήθεια του κυματικού μοντέλου SWAN σε ένα σχετικά ορθογώνιο πυκνό πλέγμα. Οι αρχικές συνθήκες (ταχύτητα και διεύθυνση ανέμου) για μια παρελθοντική περίοδο θα προκύψουν από τα δεδομένα reanalysis NCEP/NCAR..

# Chapter 1

## Introduction

In the scientific community of coastal engineering, wind-waves are the most important phenomenon to be considered among the environmental conditions affecting maritime structures and other marine and coastal activities. Nevertheless, wind waves have very complex natures. Looking out at the sea, one never sees a constant progression of identical waves. On second thought, the sea surface is composed of waves of varying heights and periods moving in different directions. Moreover, wind waves are highly irregular with respect to their direction, amplitude and frequency and generally they have random nature.

Nowadays, a crucial topic of our society is that disasters and their impact on human populations have been increased rapidly. A fundamental reason of this vital situation is the Climate change. This is a modification in the distribution of climate patterns making risks increasingly challenging to predict and changing the ways in which hazards interact with each other. Actions of humans have been identified as vital causes of recent global warming. The factors causing climate change are natural, external and anthropogenic, and the impacts are felt in land, water and atmosphere. Coastal zones are important for humans because they have special characteristics like warm weather, productive soils and more job opportunities that provide a better life quality.

In the sense of macroscopic application, the biggest motivation for developing wind driven wave models is to predict the behavior of the ocean surface throughout different weather events over time. Thus, the behavior of the ocean surface is substantial for many reasons, some relevant from an engineering standpoint and others relevant from a personal standpoint. A singular person might want to know future ocean wave behavior for safety purposes related to surfing or boating, whilst the engineer seeks to model the behavior of the water body in an effort to relate it to weather safety, shore infrastructure or other fluid related design.

For this reason, wave models are commonly used by government organizations such as NOAA (National Oceanic and Atmospheric Administration) and FEMA (Federal Emergency Management Agency). These organizations often utilize wave models as a component of comprehensive ocean and lake modeling to simulate past

or future events with extreme weather circumstances in order to better understand issues such as structural damage, flooding, pollution transport, or erosion. Instances of these situations are disasters such as hurricanes, tsunamis, or oil spills; all of which benefit from both forecast and hind cast simulations to increase scientific knowledge about the event. In order to accurately simulate these events, wave models are coupled with other models that add additional detail to the simulation.

SHYFEM (Shallow water Hydrodynamic Finite Element Model), [3], has been developed at ISMAR-CNR (Institute of Marine Sciences - National Research Council; Umgiesser, 2004) and been already and successfully applied to several coastal environments. This forecasting model can be used to resolve the hydrodynamic equations in lagoons, coastal seas, estuaries and lakes. It consists of a 3D shallow water hydrodynamic model, coupled with a wind wave model and with both an Eulerian and a Lagrangian module, for simulating active tracers transport and diffusion. The model resolves the shallow water equations in their formulations with water levels and transports. The finite element method permits to reproduce complex morphologies and bathymetries. This program accounts for both barotropic and baroclinic pressure gradients, wind drag forcing, bottom friction dissipation, Coriolis forcing and wind wave forcing.

Some limitations that are inherited from the SWE assumptions are: a) that it is possible to use these equations only in the case where the horizontal wave length is much greater than the vertical length scale and b) that since the SWE have only one vertical level, they cannot account for any factor varying in the water depth.

MIKE 21 was developed by DHI (Danish Hydraulic Institute) Water Environment Health and it is used to simulate physical, chemical and biological processes in coastal and marine waters (DHI webpage, 2011). MIKE 21 is designed for 2D free surface modelling of flow and waves; sediment transport and environmental processes for estuaries and coastal applications.

MIKE is composed of two different modules:

- A Spectral Waves Module (SWM), which is a fully spectral formulation based on the work of Komen and Young in [17] and [24] respectively. The solution is achieved by an unstructured cell-centered finite volume method in two dimensions with triangles or quadrilaterals and the time integration is performed by an explicit fractional step method. The governing equation is the wave action balance equation in cartesian coordinates,
- A Hydrodynamic Module (HDM) solving the NavierStokes equations under the Boussinesq and hydrostatic pressure assumptions on a structured or unstructured cell-centered finite volume grid in 2D

The limitations of this model are that according to experienced users special care needs to be taken for the drying grid cells on the open boundaries and different approaches have been developed to overcome some inherent weaknesses of

the model. Another rather common issue refers to the artificial backwater effects from the boundaries. However, that can be easily minimized by allowing enough distance from the boundaries to the region of interest in the computational domain.

Delft3D is a software suite developed by Deltares, formerly known as Delft Hydraulics, for 3D computations in coastal, river and estuarine areas. It covers numerical modelling of flows, sediment transport, waves, water quality, morphological developments and ecology. Delft3D is composed of several modules which can be executed independently or can be coupled together and interact with one another, by exchanging information automatically via the communication file. Delft3D-FLOW, [1], is one of these modules, which is a program used for 2D (depth-averaged) or 3D hydrodynamic and transport simulations. It can calculate non-steady flow and transport phenomena caused by tidal and meteorological forcing on a rectilinear or curvilinear boundary fitted grid.

As a numerical model, Delft3D-FLOW follows all the restrictions embedded in a model. That means that the solution produced is only an approximation of the exact solution and the accuracy is subject to the numerical schemes used, to the discretization of the bottom topography and the assumptions made on the physical processes. Moreover, the time integration influences the wave propagation. The limitation here is that free surface waves can be propagated correctly only when a small time step is selected. In this case, the computational cost increases significantly.

In the present study, the characteristics of the waves, current velocities, depth averaged velocity, horizontal velocity and water level of sea surface are simulated for forecast and hindcast in Thracian Sea, using a modeling procedure within the Delft3D model.

Furthermore, the results are compared with other measurements in this area. The main objectives are to:

- Fine tune the coupling of the particular models included in Delft3D, regarding the appropriate selection of the artificial boundaries and its conditions, the hierarchy of nested grids and appropriate modeling of the outer wave problem.
- Estimate the hydrodynamic conditions of the event.
- Estimate the accuracy of the numerical modeling in relation with the real data.

For the simulation, the numerical model of the open source code of Delft3D was used. With Delft3d, the calculation of the wave field in relation with the hydrodynamics is the product of the coupling of two models, that of the Delft3d-WAVE model, [2], and that of the Delft3d-FLOW model, [1], respectively.

This study is presented in the subsequent chapters as follows: In chapter 2, a brief description of the Delft3D model is given. In chapter 3, the data analysis

through copernicus cmems system and R programming language are described. In chapter 4, the case study and the model setup are presented with the results of the computations and comparisons with the measurements obtained. Finally, the conclusions are discussed.

# Chapter 2

## Description of the Delft3D model

The Delft3D model is developed for a multi-disciplinary approach to nearshore waves and morphodynamic modeling by Deltares <sup>1</sup>, in close cooperation with Delft University of Technology. Delft3D consists of several models that can interact with each other. The Delft3D-FLOW simulates the hydrodynamic phenomena, the sediment transport processes and the bottom changes and the Delft3D-WAVE simulates the wave generation and propagation in nearshore areas.

Delft3D-FLOW is the hydrodynamic module of Delft3D, which is Delft Hydraulics' fully integrated program for the modelling of water flows, waves, water quality, particle tracking, ecology, sediment and chemical transports and morphology. In Figure 1 a system overview of Delft3D is given.

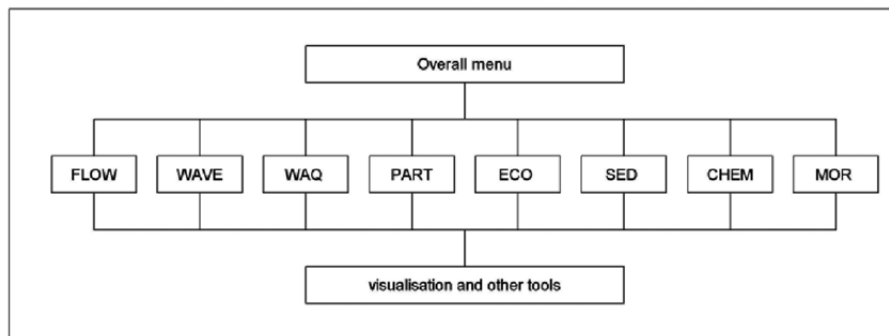


Figure 2.1: System overview of Delft3D

We note that in previous versions of Delft3D also contained a MOR(phology) module. However, the morphology functionality is now part of the FLOW module and a separate MOR module does not exist anymore.

The primary purpose of the computational model Delft3D-FLOW is to solve various one-, two and three-dimensional, time-dependent, non-linear differential equations related to hydrostatic and non-hydrostatic free-surface flow problems on a structured orthogonal grid to cover problems with complicated geometry. The equations are formulated in orthogonal curvilinear co-ordinates on a plane or in spherical co-ordinates on the globe. In Delft3D-FLOW models with a rectangular

---

<sup>1</sup>Deltares is an independent institute for applied research in the field of water, subsurface and infrastructure.

or spherical grid (Cartesian frame of reference) are considered as a special form of a curvilinear grid, see [Kernkamp et al., 2005] and [Willemse et al., 1986].

The equations solved are mathematical descriptions of physical conservation laws for:

- water volume (continuity equation),
- linear momentum (Reynolds-averaged Navier-Stokes (RANS) equations), and
- tracer mass (transport equation) , e. g. for salt, heat (temperature) and suspended sediments or passive pollutants.

Furthermore, bed level changes are computed, which depend on the quantity of bottom sediments.

The following physical quantities can be obtained in dependence on three-dimensional space  $(x,y,z)$  and time  $t$ :

- water surface elevation  $\zeta(x,y,z,t)$  with regard to a reference surface (e. g. mean sea level),
- current velocity  $u(x,y,z,t)$ ,  $v(x,y,z,t)$ ,  $w(x,y,z,t)$ ,
- non-hydrostatic pressure component  $q(x,y,z,t)$ ,
- tracer concentration  $C(x,y,z,t)$ , e. g. temperature, salinity, concentration of suspended sediments or passive pollutants; and
- bed level  $d(x,y,t)$ , representing changes in bathymetry.

Delft3D-FLOW can be used in either hydrostatic or non-hydrostatic mode. In case of hydrostatic modelling the so-called shallow water equations are solved, whereas in nonhydrostatic mode the Navier-Stokes equations are taken into account by adding nonhydrostatic terms to the shallow water equations. A fine horizontal grid is needed to resolve non-hydrostatic flow phenomena. When the computational model Delft3D-FLOW is used in one- or two-dimensional mode (with one  $z$ -layer in vertical direction) the results for  $u$ ,  $v$  and  $C$  will be the respective depth averaged values for current velocity and tracer concentration.

For the vertical grid system two options are available in Delft3D-FLOW, namely so-called  $\sigma$ - or  $z$ -coordinates.

### **Vertical grid**

3D numerical modelling of the hydrodynamics and water quality in these areas requires accurate treatment of the vertical exchange processes. The existence of vertical stratification influences the turbulent exchange of momentum, heat, salinity and passive contaminants. The accuracy of the discretisation of the vertical exchange processes is determined by the vertical grid system. The vertical grid should:

- resolve the boundary layer near the bottom and surface to allow an accurate evaluation of the bed stress and surface stresses, respectively;
- be fine around pycnoclines;
- avoid large truncation errors in the approximation of strictly horizontal gradients.

The two commonly used vertical grid systems in 3D shallow-water models are the  $z$  coordinate system (Z-model) and the so-called  $\sigma$ -coordinate system ( $\sigma$ -model). Neither meets all the requirements. The Z-model has horizontal coordinate lines which are (nearly) parallel with isopycnals, but the bottom is usually not a coordinate line and is represented instead as a staircase (zig-zag boundary). This leads to inaccuracies in the approximation of the bed stress and the horizontal advection near the bed. The sigma-model has quasi-horizontal coordinate lines. The first and last grid line follow the free surface ( $\sigma = 0$ ) and the sea bed boundary ( $\sigma = -1$ ), respectively, with a user defined  $\sigma$ -distribution in between. The grid lines follow the bottom topography and the surface but generally not the isopycnals. Inaccuracies associated with these numerical artefacts have been addressed in Delft3D, which has led to acceptable solutions for practical applications. In Delft3D-FLOW both the options of fixed horizontal layers (Z-model) and the sigma grid ( $\sigma$ -model) are operational. The two grid concepts are illustrated in Figure 2.

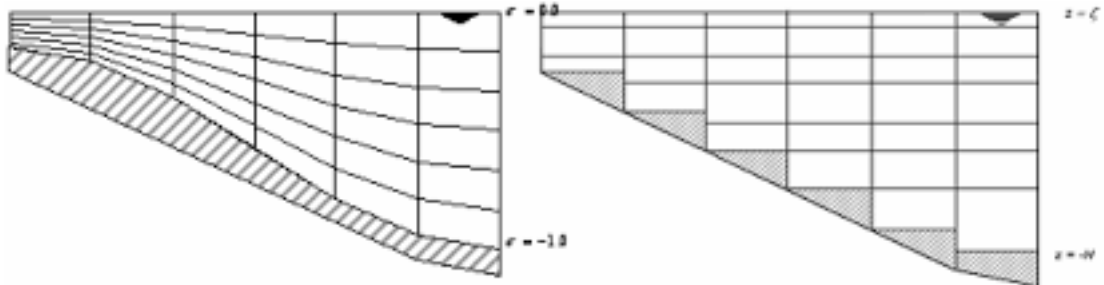


Figure 2.2:  $\sigma$ -model and  $z$ -coordinate model

In practice, this means that depending on the application the user can choose the best option for the representation of the processes in the vertical. In case of stratified flow problems in coastal seas, estuaries and lakes where steep topography is a dominant feature, this is an important issue. For lakes a Z-model is preferred, because the vertical exchange process should not be dominated by truncation errors.

In this study, the wave-driven longshore currents are modeled by the interaction between Delft3D-FLOW and Delft3D-WAVE . The coupling of those models allow a two way exchange of information between them, so as the effect of waves on currents and the effect of ow on waves to be accounted for. More specifically, the

wave-current interaction is implemented by running the wave module every  $N$  flow timesteps, where updated bottom, water level and velocity information are passed to the wave model and wave-induced forces, wave heights, periods and directions are passed back to the flow module (Lesser et. al., 2004).

## 2.1 Physical processes

The numerical hydrodynamic modelling system Delft3D-FLOW solves the unsteady shallow water equations in two (depth-averaged) or in three dimensions. The system of equations consists of the horizontal equations of motion, the continuity equation, and the transport equations for conservative constituents. The equations are formulated in orthogonal curvilinear co-ordinates or in spherical co-ordinates on the globe. In Delft3D-FLOW models with a rectangular grid (Cartesian frame of reference) are considered as a simplified form of a curvilinear grid. In curvilinear co-ordinates, the free surface level and bathymetry are related to a flat horizontal plane of reference, whereas in spherical co-ordinates the reference plane follows the Earth's curvature.

The flow is forced by tide at the open boundaries, wind stress at the free surface, pressure gradients due to free surface gradients (barotropic) or density gradients (baroclinic). Source and sink terms are included in the equations to model the discharge and withdrawal of water.

## 2.2 The Delft3D - FLOW model

The Delft3D-FLOW model solves the unsteady shallow-water equations for an incompressible fluid. They are derived from the Navier - Stokes equations under the Boussinesq and the shallow water assumptions.

According to the Boussinesq approximation (Rodi, 1993), if density variations are small the density is assumed constant in all terms except the gravitational term. Under this approximation, the continuity equation and Navier - Stokes equations are written in the form:

$$\frac{\partial u}{\partial x} + \frac{\partial v}{\partial y} + \frac{\partial w}{\partial z} = 0 \quad (2.1)$$

$$\begin{aligned} \frac{\partial u}{\partial t} + u \frac{\partial u}{\partial x} + v \frac{\partial u}{\partial y} + w \frac{\partial u}{\partial z} &= -\frac{1}{\rho_0} \frac{\partial p}{\partial x} + \nu \Delta u - f_x \\ \frac{\partial v}{\partial t} + u \frac{\partial v}{\partial x} + v \frac{\partial v}{\partial y} + w \frac{\partial v}{\partial z} &= -\frac{1}{\rho_0} \frac{\partial p}{\partial y} + \nu \Delta v - f_y \end{aligned} \quad (2.2)$$

$$\frac{\partial w}{\partial t} + u \frac{\partial w}{\partial x} + v \frac{\partial w}{\partial y} + w \frac{\partial w}{\partial z} = -\frac{1}{\rho_0} \frac{\partial p}{\partial z} + \nu \Delta w - f_z - \frac{\rho}{\rho_0} g$$

where  $u, v, w$  are the velocity components in  $x, y, z$  direction respectively,  $p$  is the pressure,  $\rho$  is the density,  $\rho_0$  is the reference density,  $\nu = \frac{\mu}{\rho}$  the kinematic viscosity

with  $\mu$  the dynamic or absolute viscosity and  $f_x, f_y, f_z$  denote the components of Coriolis forces per unit mass, which are defined by :

$$(f_x, f_y, f_z)^T = -2\vec{\Omega} \times (u, v, w)^T$$

where  $\vec{\Omega}$  is the vector of earth's rotation.

By hand of a time-averaging of the Navier-Stokes equations and the continuity equation for incompressible fluids, the basic equations for the averaged turbulent flow will be derived in the sequel. The flow field can then be described only with help of the mean values. In order to be able to take a time-average, the momentary value is decomposed into the parts mean value and fluctuating value. This is shown graphically in Figure 3.

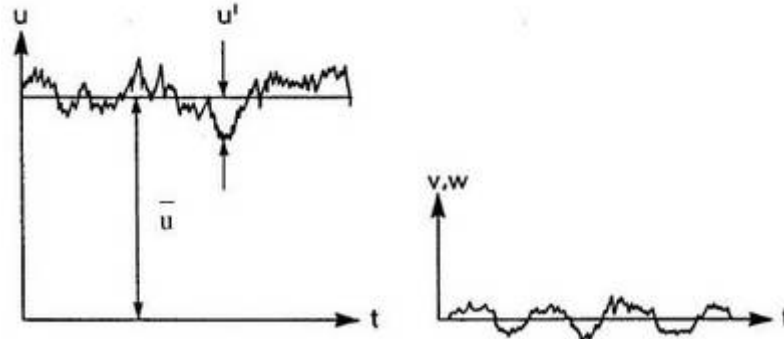


Figure 2.3: Turbulent velocity fluctuation in pipe flow as a function of time, taken from [Fredsoe, 1990].

The momentary velocity components is  $u$ , the time-averaged value is named  $\bar{u}$  and the fluctuating velocity has the letter  $u'$ . With help of this definition the decomposition can mathematically be written as:

$$u = \bar{u} + u', \quad v = \bar{v} + v', \quad w = \bar{w} + w', \quad p = \bar{p} + p', \quad f = \bar{f} + f' \quad (2.3)$$

The chosen averaging method takes the mean values at a fix place in space and averaged over a time span that is large enough for the mean values to be independent of it.

$$\bar{u} = \frac{1}{\Delta t} \int_{t_0}^{t_0 + \Delta t} u dt$$

The time-averaged values of the fluctuating values are defined to be zero:

$$\bar{u}' = 0, \quad \bar{v}' = 0, \quad \bar{w}' = 0, \quad \bar{p}' = 0$$

From eq.(2.3) and the continuity equation eq.(2.1) we get :

$$\frac{\partial \bar{u}}{\partial x} + \frac{\partial u'}{\partial x} + \frac{\partial \bar{v}}{\partial y} + \frac{\partial v'}{\partial y} + \frac{\partial \bar{w}}{\partial z} + \frac{\partial w'}{\partial z} = 0 \quad (2.4)$$

The time-average of the last equation is written as:

$$\overline{\frac{\partial \bar{u}}{\partial x} + \frac{\partial u'}{\partial x} + \frac{\partial \bar{v}}{\partial y} + \frac{\partial v'}{\partial y} + \frac{\partial \bar{w}}{\partial z} + \frac{\partial w'}{\partial z}} = 0 \quad (2.5)$$

Furthermore, we introduce some rules for time-averaging :

$$\overline{\frac{\partial \bar{u}}{\partial x}} = \frac{1}{\Delta t} \int_{t_0}^{t_0+\Delta t} \frac{\partial u}{\partial x} dt = \frac{\partial}{\partial x} \frac{1}{\Delta t} \int_{t_0}^{t_0+\Delta t} u dt = \frac{\partial \bar{u}}{\partial x}$$

$$\overline{\frac{\partial u'}{\partial x}} = \frac{1}{\Delta t} \int_{t_0}^{t_0+\Delta t} \frac{\partial u'}{\partial x} dt = \frac{\partial}{\partial x} \frac{1}{\Delta t} \int_{t_0}^{t_0+\Delta t} u' dt = \frac{\partial u'}{\partial x} = 0$$

$$\overline{\bar{f}} = \bar{f}, \quad \overline{\bar{f} + \bar{g}} = \bar{f} + \bar{g}, \quad \overline{\bar{f} \cdot \bar{g}} = \bar{f} \cdot \bar{g}, \quad \overline{\int f ds} = \int \bar{f} ds$$

But  $\overline{\bar{f} \cdot \bar{g}} \neq \bar{f} \cdot \bar{g}$

According to these rules, the averaged derivatives of the fluctuations are also zero. Thus, the time-averaged continuity equation is:

$$\frac{\partial \bar{u}}{\partial x} + \frac{\partial \bar{v}}{\partial y} + \frac{\partial \bar{w}}{\partial z} = 0 \quad (2.6)$$

We introduce a small transformation of the advection term from eq. (2.2), and Navier-Stokes equations will be time-averaged:

$$\begin{aligned} u \frac{\partial u}{\partial x} + v \frac{\partial u}{\partial y} + w \frac{\partial u}{\partial z} &= \frac{\partial(u^2)}{\partial x} + \frac{\partial(uv)}{\partial y} + \frac{\partial(uw)}{\partial z} - \underbrace{u \left( \frac{\partial u}{\partial x} + \frac{\partial v}{\partial y} + \frac{\partial w}{\partial z} \right)}_{=0} \\ &= \frac{\partial(u^2)}{\partial x} + \frac{\partial(uv)}{\partial y} + \frac{\partial(uw)}{\partial z} \end{aligned}$$

After averaging eq.(2.2) and the above transformation, the Reynolds-averaged Navier-Stokes equations or simply the Reynolds equations for turbulent flows are obtained. They read :

$$\frac{\partial \bar{u}}{\partial t} + \bar{u} \frac{\partial \bar{u}}{\partial x} + \bar{v} \frac{\partial \bar{u}}{\partial y} + \bar{w} \frac{\partial \bar{u}}{\partial z} + \frac{\partial \overline{u'u'}}{\partial x} + \frac{\partial \overline{u'v'}}{\partial y} + \frac{\partial \overline{u'w'}}{\partial z} = -\frac{1}{\rho_0} \frac{\partial \bar{p}}{\partial x} - \bar{f}_x \quad (2.7)$$

$$\frac{\partial \bar{v}}{\partial t} + \bar{u} \frac{\partial \bar{v}}{\partial x} + \bar{v} \frac{\partial \bar{v}}{\partial y} + \bar{w} \frac{\partial \bar{v}}{\partial z} + \frac{\partial \overline{v'u'}}{\partial x} + \frac{\partial \overline{v'v'}}{\partial y} + \frac{\partial \overline{v'w'}}{\partial z} = -\frac{1}{\rho_0} \frac{\partial \bar{p}}{\partial y} - \bar{f}_y \quad (2.8)$$

$$\frac{\partial \bar{w}}{\partial t} + \bar{u} \frac{\partial \bar{w}}{\partial x} + \bar{v} \frac{\partial \bar{w}}{\partial y} + \bar{w} \frac{\partial \bar{w}}{\partial z} + \frac{\partial \overline{w'u'}}{\partial x} + \frac{\partial \overline{w'v'}}{\partial y} + \frac{\partial \overline{w'w'}}{\partial z} = -\frac{1}{\rho_0} \frac{\partial \bar{p}}{\partial z} - \bar{f}_z - \frac{\rho}{\rho_0} g \quad (2.9)$$

The products of the fluctuating velocity components ( $\overline{u'u'}$ ,  $\overline{u'v'}$  etc.) are called Reynolds stresses and they are responsible for a loss of momentum in the mean flow direction. These stresses are much larger than the viscous stresses which have been neglected for this reason.

Furthermore, according to the Boussinesq hypothesis (eddy viscosity concept), Reynolds stresses, like viscous stresses, depend on the deformation of the mean flow. Thus, the Reynolds stresses can be modeled as

$$\overline{u'u'} = -\nu_t \left( \frac{\partial \bar{u}}{\partial x} + \frac{\partial \bar{u}}{\partial x} \right) \quad (2.10)$$

$$\overline{u'v'} = -\nu_t \left( \frac{\partial \bar{v}}{\partial x} + \frac{\partial \bar{u}}{\partial y} \right) \quad (2.11)$$

$$\overline{u'w'} = -\nu_t \left( \frac{\partial \bar{u}}{\partial z} + \frac{\partial \bar{w}}{\partial x} \right) \quad (2.12)$$

where  $\nu_t$  is the eddy viscosity and is determined with a suitable closure problem for the turbulence modeling.

The shallow water assumption implies that the flow satisfies certain characteristic relations (Jin, 1993). These relations are the following :

1. The characteristic horizontal length scale is much larger than the characteristic vertical length scale.
2. The characteristic vertical velocity is small in comparison with the characteristic horizontal velocity

Under this assumption, the difference between the horizontal and the vertical length scale justifies a distinction between a horizontal ( $\nu_t^H$ ) and a vertical ( $\nu_t^V$ ) eddy viscosity. Also, all the terms except the pressure derivative and the gravity term are small, so they can be neglected. The momentum equation in the vertical direction reduces to the hydrostatic pressure distribution:

$$\frac{\partial \bar{p}}{\partial z} = -\rho g \quad (2.13)$$

i.e. by integrating

$$p(x, y, z, t) = g \int_z^\zeta \rho dz' + p_\alpha \quad (2.14)$$

where  $\zeta = \zeta(x, y, z, t)$  is the free surface level against the reference plane  $z = 0$  and  $p_\alpha$  is the atmospheric pressure. Substituting this result in the pressure term of equation (2.7) and using Leibniz integral rule <sup>2</sup>, yields

---

<sup>2</sup>The Leibniz integral rule:

$$\frac{\partial}{\partial x} \int_{\alpha(x)}^{b(x)} \phi(x, y) dy = \int_{\alpha(x)}^{b(x)} \frac{\partial}{\partial x} \phi(x, y) dy + \phi(x, b) \frac{\partial b}{\partial x} - \phi(x, \alpha) \frac{\partial \alpha}{\partial x}$$

$$-\frac{1}{\rho_0} \frac{\partial \bar{p}}{\partial x} = -\frac{\rho g}{\rho_0} \frac{\partial \zeta}{\partial x} - \frac{g}{\rho_0} \int_z^\zeta \frac{\partial p}{\partial x} dz' - \frac{1}{\rho_0} \frac{\partial p_\alpha}{\partial x} \quad (2.15)$$

The horizontal pressure gradient is described by differences of the water level  $\zeta$  through the barotropic term (gradient of the free surface level) and by the density differences in horizontal direction through the baroclinic term (second term). The last term describes the contribution of the atmospheric pressure.

If we consider  $\rho = \rho_0$  (constant), then (2.14) reads as  $\bar{p}(x, y, z, t) = \rho g(\zeta(x, y, z, t) + p_\alpha)$  and for the pressure terms of (2.7) and (2.8) we have

$$-\frac{1}{\rho_0} \frac{\partial \bar{p}}{\partial x} = g \frac{\partial \zeta}{\partial x} + \frac{1}{\rho_0} \frac{\partial p_\alpha}{\partial x} \quad (2.16)$$

and

$$-\frac{1}{\rho_0} \frac{\partial \bar{p}}{\partial y} = g \frac{\partial \zeta}{\partial y} + \frac{1}{\rho_0} \frac{\partial p_\alpha}{\partial y} \quad (2.17)$$

respectively.

In large bodies of water (eg coastal waters, estuaries), universal forces must be included in addition to the force of gravity and the Coriolis force that expresses the effect of the earth's rotation. Considering the x,y axes of the Cartesian coordinate system horizontally and the z vertical axis upwards, the components of the universal forces  $f_x, f_y, f_z$  are given by the following relationships:

$$f_x = fv, \quad f_y = -fu, \quad f_z = -g$$

where  $f = 2\Omega \sin \phi$  is the Coriolis force with  $\Omega$  to represent the angular velocity of the earth and  $\phi$  the latitude.

Considering the above assumptions, the density and the atmospheric pressure to be constant and dropping the overbar, equations (2.7) and (2.8) are, respectively, transformed into:

$$\begin{aligned} & \frac{\partial u}{\partial t} + u \frac{\partial u}{\partial x} + v \frac{\partial u}{\partial y} + w \frac{\partial u}{\partial z} = \\ & -g \frac{\partial \zeta}{\partial x} + fv + 2 \frac{\partial \left( \nu_t^H \frac{\partial u}{\partial x} \right)}{\partial x} + \frac{\partial \left( \nu_t^H \left( \frac{\partial u}{\partial y} + \frac{\partial v}{\partial x} \right) \right)}{\partial y} + \frac{\partial \left( \nu_t^V \frac{\partial u}{\partial z} \right)}{\partial z} \end{aligned} \quad (2.18)$$

$$\begin{aligned} & \frac{\partial v}{\partial t} + u \frac{\partial v}{\partial x} + v \frac{\partial v}{\partial y} + w \frac{\partial v}{\partial z} = \\ & -g \frac{\partial \zeta}{\partial y} - fu + \frac{\partial \left( \nu_t^H \left( \frac{\partial u}{\partial y} + \frac{\partial v}{\partial x} \right) \right)}{\partial x} + 2 \frac{\partial \left( \nu_t^H \frac{\partial v}{\partial y} \right)}{\partial y} + \frac{\partial \left( \nu_t^V \frac{\partial v}{\partial z} \right)}{\partial z} \end{aligned} \quad (2.19)$$

The above equations together with the incompressible continuity equation

$$\frac{\partial u}{\partial x} + \frac{\partial v}{\partial y} + \frac{\partial w}{\partial z} = 0 \quad (2.20)$$

are the so-called Shallow Water Equations.

In order to obtain the third equation that is needed for calculating the four unknowns  $(u, v, w, \zeta)$ , the continuity equation is integrated along the vertical axis:

$$\omega(x, y, \zeta, t) - \omega(z, y, d, t) = - \int_{-d}^{\zeta} \frac{\partial u}{\partial x} dz - \int_{-d}^{\zeta} \frac{\partial v}{\partial y} dz \quad (2.21)$$

where  $d = d(x, y)$  is the water depth below the reference plane  $z = 0$ . For the water level ( $z = \zeta(x, y, t)$ ) and for the bottom ( $z = -d(x, y)$ ) respectively,

$$\omega = \frac{D\zeta}{Dt} = \frac{\zeta}{\partial t} + u \frac{\zeta}{\partial x} + v \frac{\zeta}{\partial y} \quad (2.22)$$

$$\omega = -u \frac{\partial d}{\partial x} - v \frac{\partial d}{\partial y} \quad (2.23)$$

We apply the Leibniz integral rule:

$$- \int_{-d}^{\zeta} \frac{\partial u}{\partial x} dz = - \frac{\partial u}{\partial x} \int_{-d}^{\zeta} dz + u \frac{\zeta}{\partial x} + u \frac{\partial d}{\partial x}$$

and

$$- \int_{-d}^{\zeta} \frac{\partial v}{\partial y} dz = - \frac{\partial v}{\partial y} \int_{-d}^{\zeta} dz + v \frac{\zeta}{\partial y} + v \frac{\partial d}{\partial y} \quad (2.24)$$

(2.21) yields:

$$\frac{\partial \zeta}{\partial t} = - \frac{\partial u}{\partial x} \int_{-d}^{\zeta} dz - \frac{\partial v}{\partial y} \int_{-d}^{\zeta} dz \quad (2.25)$$

Defining depth-averaged velocities as  $\bar{u} = \frac{1}{H} \int_{-d}^{\zeta} u dz$  and  $\bar{v} = \frac{1}{H} \int_{-d}^{\zeta} v dz$  respectively, where  $H = H(x, y, t) = \zeta + d$  is the water depth.

Finally, we can use our boundary conditions to get the rid of the boundary terms. Thus, from the equation (2.25), the depth averaged continuity equation is

$$\frac{\partial \zeta}{\partial t} + \frac{\partial H \bar{u}}{\partial x} + \frac{\partial H \bar{v}}{\partial y} = 0 \quad (2.26)$$

The hydrodynamic equations are solved on a Cartesian, rectangular grid. In 3D simulations, a boundary fitted ( $\sigma$ - coordinate) approach is used for the vertical grid direction.

The  $\sigma$ -coordinate system is a boundary fitted coordinate system that follows the free surface and the bottom topography. Such a coordinate system allows for

non - uniformly distributed grid lines on the computational domain, especially near the bottom, where a proper forecasting of the sediment transport requires the grid lines to be dense and therefore to increase the resolution.

In the following, the complex physical domain for the shallow water equations 2.18, 2.19, 2.20 and 2.26 is transformed to a rectangular computational domain by introducing the  $\sigma$ -coordinates system

$$\tilde{x} = x, \quad \tilde{y} = y, \quad \sigma = \frac{z - \zeta}{d + \zeta} = \frac{z - \zeta}{H}, \quad \tilde{t} = t \quad (2.27)$$

where:

$z$  = the vertical coordinate in physical space

$\zeta$  = the free surface elevation above the reference plane ( $z=0$ )

$d$  = the depth below the reference plane

$H$  = the total water depth

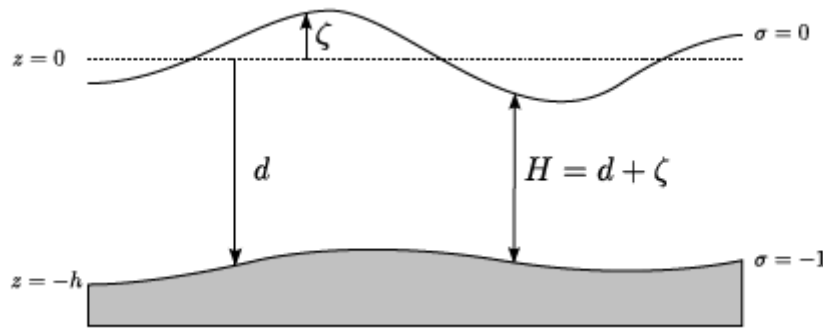


Figure 2.4: Definition of water level ( $\zeta$ ), depth( $h$ ) and total depth ( $H$ ), taken from manual delft3D-Flow.

At the bottom  $\sigma = 1$  and at the free surface  $\sigma = 0$ . The flow domain of a 3D shallow water model in the horizontal plane consists of a restricted (limited) area composed of open and closed (land) boundaries and in the vertical of a number layers, which is the same at every location. For each layer, a system of equations is solved.

The partial derivatives are expressed in  $\sigma$ - coordinates by the chain rule, introducing additional terms (Stelling et. al., 1994).

The time derivative in  $\sigma$ -coordinates reads:

$$\frac{\partial}{\partial t} = \frac{\partial}{\partial \tilde{t}} + \frac{\partial \sigma}{\partial \tilde{t}} \frac{\partial}{\partial \sigma}$$

The spatial derivatives in the horizontal direction are:

$$\frac{\partial}{\partial x} = \frac{\partial}{\partial \tilde{x}} + \frac{\partial \sigma}{\partial \tilde{x}} \frac{\partial}{\partial \sigma}, \quad \frac{\partial}{\partial y} = \frac{\partial}{\partial \tilde{y}} + \frac{\partial \sigma}{\partial \tilde{y}} \frac{\partial}{\partial \sigma}$$

In the vertical direction are:

$$\frac{\partial}{\partial z} = \frac{1}{H} \frac{\partial}{\partial \sigma}$$

Equation (2.13) in  $\sigma$ - coordinates reads:

$$\frac{\partial \tilde{p}}{\partial \sigma} = -\rho g H \quad (2.28)$$

After integrating along the vertical axis we obtain the hydrostatic pressure :

$$\tilde{p} = gH \int_{\sigma}^0 \rho(x, y, \sigma', t) d\sigma' + p_{\alpha} \quad (2.29)$$

The horizontal velocities  $u$  and  $v$  remain strictly horizontal after the transformation

$$\tilde{u} = u, \quad \tilde{v} = v$$

Considering that, the vertical velocity becomes

$$\begin{aligned} \tilde{\omega} &:= H \frac{D\sigma}{Dt} \\ \tilde{\omega} &= H \left[ \frac{\partial}{\partial t} \left( \frac{z - \zeta}{H} \right) + u \frac{\partial}{\partial x} \left( \frac{z - \zeta}{H} \right) + v \frac{\partial}{\partial y} \left( \frac{z - \zeta}{H} \right) \right] \\ \tilde{\omega} &= \omega - \left( \frac{\partial \zeta}{\partial t} + u \frac{\partial \zeta}{\partial x} + v \frac{\partial \zeta}{\partial y} \right) - \sigma \left( \frac{\partial H}{\partial t} + u \frac{\partial H}{\partial x} + v \frac{\partial H}{\partial y} \right) \end{aligned} \quad (2.30)$$

From this, the (comparatively small) vertical velocity  $w$  can be expressed in the  $(x, y, z)$  coordinates, in terms of the horizontal velocities, water depths, water levels and vertical  $\sigma$ - velocities, as

$$\omega = \tilde{\omega} + u \left( \sigma \frac{\partial H}{\partial x} + \frac{\partial \zeta}{\partial x} \right) + v \left( \sigma \frac{\partial H}{\partial y} + \frac{\partial \zeta}{\partial y} \right) + \left( \sigma \frac{\partial H}{\partial t} + \frac{\partial \zeta}{\partial t} \right)$$

After substituting (2.30) into the continuity equation (2.20), assuming that  $d$  is not time dependent and noting that  $H$  and  $\zeta$  are not  $\sigma$ -dependent, whereas  $u$  and  $v$  are, the continuity equation in transformed coordinates is obtained:

$$\frac{\partial \zeta}{\partial \tilde{t}} + \frac{\partial H \tilde{u}}{\partial \tilde{x}} + \frac{\partial H \tilde{v}}{\partial \tilde{y}} + \frac{\partial \omega}{\partial \sigma} = 0 \quad (2.31)$$

The vertical velocities can be computed by integrating equation 2.31 from the bottom to the surface ( $-1 \leq \sigma \leq 0$ ) and using Leibniz' integral rule:

$$\frac{\partial \zeta}{\partial \tilde{t}} + \frac{\partial H \tilde{u}}{\partial \tilde{x}} + \frac{\partial H \tilde{v}}{\partial \tilde{y}} = 0 \quad (2.32)$$

where  $\bar{u}$  and  $\bar{v}$  are depth-averaged velocities defined by  $\bar{u} = \int_{-1}^0 \tilde{u} d\sigma$  and  $\bar{v} = \int_{-1}^0 \tilde{v} d\sigma$ . Note that, this equation is equal to (2.26) in the previous section, because it is integrated along the vertical axis and therefore invariant under the  $\sigma$ -transformation. Also, the definitions of  $\bar{u}$  and  $\bar{v}$  are equivalent to the definitions

in the previous section.

After transformation of (2.18) and (2.19) to  $\sigma$ -coordinates, the momentum equations in x- and y-direction of the shallow-water equations, omitting the overbar, are given by:

$$\begin{aligned} & \frac{\partial u}{\partial t} + u \frac{\partial u}{\partial x} + v \frac{\partial u}{\partial y} + \frac{w}{H} \frac{\partial u}{\partial z} = \\ & - \frac{1}{\rho_0} \left( \frac{\partial p}{\partial x} + \frac{\partial \sigma}{\partial x} \frac{\partial p}{\partial \sigma} \right) + fv + F_x + M_x + \frac{1}{H^2} \frac{\partial}{\partial \sigma} \left( \nu_t^V \left( \frac{\partial u}{\partial \sigma} \right) \right) \end{aligned} \quad (2.33)$$

$$\begin{aligned} & \frac{\partial v}{\partial t} + u \frac{\partial v}{\partial x} + v \frac{\partial v}{\partial y} + \frac{w}{H} \frac{\partial v}{\partial z} = \\ & - \frac{1}{\rho_0} \left( \frac{\partial p}{\partial y} + \frac{\partial \sigma}{\partial y} \frac{\partial p}{\partial \sigma} \right) + fu + F_y + M_y + \frac{1}{H^2} \frac{\partial}{\partial \sigma} \left( \nu_t^V \left( \frac{\partial v}{\partial \sigma} \right) \right) \end{aligned} \quad (2.34)$$

$$\frac{\partial \zeta}{\partial \tilde{t}} + \frac{\partial H \tilde{u}}{\partial \tilde{x}} + \frac{\partial H \tilde{v}}{\partial \tilde{y}} + \frac{\partial \omega}{\partial \sigma} = 0 \quad (2.35)$$

The terms  $M_x$  and  $M_y$  are introduced to represent the contributions due to external sources or sinks of momentum (external forces by hydraulic structures, discharge or withdrawal of water, wave stresses, etc.).

The terms  $F_x$  and  $F_y$  represent the horizontal viscosity terms and they are given by:

$$F_x = \nu_H \left( \frac{\partial^2 u}{\partial x^2} + \frac{\partial^2 u}{\partial y^2} \right) \quad \text{and} \quad F_y = \nu_H \left( \frac{\partial^2 v}{\partial x^2} + \frac{\partial^2 v}{\partial y^2} \right) \quad (2.36)$$

where the horizontal eddy viscosity has been assumed to be a constant (Lesser et. al., 2004).

## 2.3 The Delft3D - WAVE model

The computation of waves and wave-induced effects is the domain of the wave model (Delft3D-WAVE). Delft3D -WAVE supports currently a third generation wave model, namely the SWAN model , [4], that explicitly represents all relevant physics for the development of the sea state in two dimensions (Ris, 1997).

The SWAN model is developed to simulate waves in the near-shore zone. This zone extends from the coast to several tens of kilometers into the sea. Using available input data (wind,current, water velocity), SWAN computes random, short - crested wind-generated waves in coastal regions and inland waters. The basic scientific philosophy of SWAN is identical to that of WAM cycle 3, [26]. WAM cycle 3 is presented that integrates the basic transport equation describing the evolution of a two-dimensional ocean wave spectrum without additional ad hoc assumptions

regarding the spectral shape. The three source functions describing the wind input, nonlinear transfer, and white-capping dissipation are prescribed explicitly. An additional bottom dissipation source function and refraction terms are included in the finite-depth version of the model. The model was calibrated against fetch-limited wave growth data. Only two tuning parameters are introduced in the white-capping dissipation source function. SWAN is also a third-generation wave model and it uses the same formulations for the source terms.

### 2.3.1 Wave height and period

In the description of wind waves it is common to define the wave height  $H$  as the vertical distance between the highest and the lowest surface elevation (crest to trough) in a wave. The mean wave height  $\bar{H}$  is defined as

$$\bar{H} = \frac{1}{N} \sum_{i=1}^N H_i \quad (2.37)$$

where  $H_i$  is the sequence of waves in a record. Sometimes, a quadratic weighted averaged value is used to define the root - mean - square wave height  $H_{rms}$ :

$$H_{rms} = \frac{1}{N} \left( \sum_{i=1}^N H_i^2 \right)^{\frac{1}{2}} \quad (2.38)$$

which is relevant for energy-related projects because the wave energy is proportional to the square of the wave height.

These characteristic wave heights  $\bar{H}$  and  $H_{rms}$  they are not very often used because they deviate from visual estimated wave heights. Instead, another wave height, called the significant wave height  $H_s$  is used. It is defined as the mean of the highest one - third of waves in a wave record:

$$H_s = H_{1/3} = \frac{1}{N/3} \sum_{j=1}^{N/3} H_j \quad (2.39)$$

where  $j$  is the rank number of the sorted wave heights ( $j=1$  the highest wave,  $j=2$  the second -highest, etc.).

The period  $T$  of a wave is defined as the time interval between two crests/troughs or two downward/upward zero-crossings. If the wave period is defined as the zero-crossings, it is called  $T_0$  and the mean wave period  $\bar{T}$  is defined as:

$$\bar{T} = \frac{1}{N} \sum_{i=1}^N T_{o,i} \quad (2.40)$$

Mostly, only the significant wave period is used:

$$T_s = T_{1/3} = \frac{1}{N/3} \sum_{j=1}^{N/3} T_{o,j} \quad (2.41)$$

### 2.3.2 Spectral description of wind waves

To specify fully the sea state, velocity information should be given in addition to the height of the sea surface everywhere. Moreover, to determine the time evolution one must specify the external conditions, such as wind and tides. Due to the fact that it is impossible to specify the initial state in complete detail, we use a statistical description, in which the probability of finding a particular sea state is considered. Generally, this involves knowledge of the joint probability function  $P(\eta_1, \eta_2, \dots, \eta_n)$  where

$$P(\eta_1, \eta_2, \dots, \eta_n) d\eta_1 d\eta_2 \dots d\eta_n \quad (2.42)$$

is the probability that the surface displacements  $\eta_i, i = 1, \dots, n$  (or their derivatives) at the points  $(x_i, t_i)$  have values between  $\eta_i$  and  $\eta_i + d\eta_i$ .

The probability distribution of the sea surface is nearly Gaussian, thus a good approximate description is provided by the covariance function

$$\langle \eta(x_1, t_1) \eta(x_2, t_2) \rangle, \quad (2.43)$$

the fourier transform of which is known as the wave spectrum.

The wave spectrum also has a physical meaning, because it can be shown to be the density function specifying the distribution of energy over wave components with different wave number vectors and frequencies. Its integral over all wave components is proportional to the total wave energy per unit area.

In this chapter, three-dimensional space coordinates will be denoted by  $(x_1, x_2, x_3)$ , the velocity three-vector by  $(u_1, u_2, u_3)$ , pressure by  $p(x_1, x_2, x_3, t)$ , time by  $t$  and density by  $\rho(x_1, x_2, x_3, t)$ . When it is convenient the vertical coordinate  $x_3$  and the vertical velocity component  $u_3$  will also be denoted by  $z$  and  $w$ , respectively.

An approximation to simplify the equations of air motion is to take the velocity in water as irrotational, so that the motion can be described by potential flow. In this case one introduces the velocity potential  $\phi(x_1, x_2, z, t)$  with the property :

$$u_i = \phi_{x_i}, \quad i = 1, 2, 3 \quad (2.44)$$

where we use the short hand notation for differentiation. The full nonlinear equations then read

$$\left. \begin{aligned} \phi_{x_1 x_1} + \phi_{x_2 x_2} + \phi_{x_3 x_3} &= 0, \quad z < \eta(x_1, x_2, t) \\ \eta_t + \phi_{x_1 \eta_{x_1}} + \phi_{x_2 \eta_{x_2}} &= \phi_z, \\ \phi_t + \frac{1}{2}[\phi_{x_1}^2 + \phi_{x_2}^2 + \phi_z^2] + g\eta &= 0 \end{aligned} \right\} z = \eta(x_1, x_2, t) \quad (2.45)$$

The energy of the fluid in motion is as usual the sum of potential energy and kinetic energy.

For  $\mathcal{E}$  the energy density [ $J/m^2$ ] one obtains in the potential flow description

$$\mathcal{E} = \frac{1}{2}g\rho\eta^2 + \int_{-\infty}^{\eta} \frac{1}{2}\rho[\phi_{x_1}^2 + \phi_{x_2}^2 + \phi_z^2]dz \quad (2.46)$$

where  $\rho = \rho_w$ , the density of water,  $g$  the acceleration due to gravity and  $\eta$  the interface between air and water. The total energy is given by:

$$E_{tot} = \int \int \mathcal{E} dx_1 dx_2 \quad (2.47)$$

The x-integrals extend over the total basin considered.

In any case, we can also introduce  $\tilde{\mathcal{E}}$  the energy per unit area, by dividing (2.47) by the total surface. For a basin of dimension  $L \times L$

$$\tilde{\mathcal{E}} = \frac{1}{L^2} \int \int \mathcal{E} dx_1 dx_2 \quad (2.48)$$

It is often convenient to represent  $\eta$  by a discrete Fourier representation. One way of obtaining such a representation is to subdivide the  $k_{x_1}$ - and  $k_{x_2}$ -axes into equidistant intervals with the help of a bandwidth  $\Delta k$ :

$$\eta(x, t) = \sum_k \eta_\kappa + c.c. = \sum_k \tilde{\alpha}_\kappa e^{ikx} + c.c. = \sum_k \alpha_\kappa e^{i(kx - \omega t)} + c.c., \quad (2.49)$$

with  $k = (\pm n\Delta k, \pm m\Delta k)$ ,  $n, m = 1, \dots, N_{max}$

$$\text{and } \alpha_k = \int_{k - \frac{1}{2}\Delta k}^{k + \frac{1}{2}\Delta k} \hat{\eta}(k) dk$$

The general discussion of propagation in nonhomogeneous media is more easily performed within the frame of a WKB approach<sup>3</sup>. In this approach one considers a superposition of WKB modes of the form :

$$\eta(x, t) = \sum_n \alpha_n(x, t) e^{i(k_n x - \omega_n t)} + c.c. \quad (2.50)$$

where  $\eta$  is the sea surface elevation,  $\alpha_n$  the random phase of the  $n^{th}$  wave component and  $\omega_n$  the radian frequency of the  $n^{th}$  wave component.

## The energy distribution and the wave spectrum

Substituting (2.49) in (2.48) and (2.47), the average energy per unit area can be obtained. To this end one must express  $\phi$  in terms of  $\eta$ , so that each term in (2.46) can be computed separately. In doing this one finds that the potential

---

<sup>3</sup>Is a method for finding approximate solutions to linear differential equations with spatially varying coefficients, in quantum mechanics

energy density and the kinetic energy density are not, in general, equal at a given time. This disparity occurs because there may be standing waves, for which there is a periodic exchange of energy between both terms of (2.46). With and without standing waves, the following result is obtained for the desired energy density :

$$\tilde{\mathcal{E}} = \rho g \sum_k F_k \quad (2.51)$$

where

$$F_k = 2 |\alpha_k|^2 \quad (2.52)$$

which apart from the factor  $\rho g$ , is the mean energy per Fourier mode.

We can re-express the (2.51) eq. as:

$$\tilde{\mathcal{E}} = \rho g \int F(k) dk \quad (2.53)$$

The quantity  $F(k)$  as well as its discrete counterpart  $F_k$  is known as the wave (energy) spectrum. It is of crucial and central importance in the description of ocean waves. It should be noted how much simpler equation (1.93) is than the original equation (2.46). This is because we linearized the equations and because we expanded in normal modes. The energy as given by (1.93) does not depend on time, simply because the  $\alpha_k$  do not. Now, we introduce a quantity  $N_k$  which, apart from a factor  $\rho g$ , is the wave action density per Fourier mode

$$N_k = \frac{2 |\alpha_k|^2}{\sigma_k} \quad (2.54)$$

with  $\sigma_k$  the relative frequency of the  $k^{th}$  wave component. Comparing (2.52) and (2.54) we have :

$$N_k = \frac{F_k}{\sigma} \quad (2.55)$$

It is instructive to calculate the mean wave energy  $\langle \mathcal{E} \rangle$ , from the expression given for  $\mathcal{E}$  given in (2.46), as an ensemble average. In this case the average potential and kinetic energy are equal, thus we have the simple relation :

$$\langle \mathcal{E} \rangle = \rho g \langle \eta^2 \rangle \quad (2.56)$$

and

$$\langle \eta^2 \rangle = \sum_k F_k \quad (2.57)$$

which leads to

$$\langle \mathcal{E} \rangle = \rho g \sum_k F_k \quad (2.58)$$

Comparison with (2.51) shows that the ensemble mean energy is identical with the spatially averaged energy, as indeed it must be.

Due to the irregular nature of wind, wind generated waves have irregular wave heights and periods. As a result of this irregular nature, the sea surface is continually varying, which means that a deterministic approach to describe the sea surface is not feasible. The surface elevation of waves in the ocean, at any location and any time, can be seen as the superposition of a large number of harmonic waves of different frequencies, each of which has been generated by turbulent wind in different places and times. They are therefore statistically independent in their origin. According to linear wave theory, they remain independent during their journey across the ocean. All these regular wave fields propagate at different speeds so that the appearance of the sea surface is constantly changing. Under these conditions, the sea surface elevation on a time scale of one hundred characteristic wave periods is sufficiently well described as a stationary, Gaussian process. The sea surface elevation in one point as a function of time can be described as

$$\eta(t) = \sum_i \alpha_i \cos(\sigma_i t + \alpha_i) \quad (2.59)$$

where  $\eta$  the sea surface elevation,  $\alpha_i$  the amplitude of the  $i^{th}$  wave component,  $\sigma_i$  the relative radian or circular frequency of the  $i^{th}$  wave component in the presence of the ambient current (equals the absolute radian frequency  $\omega$  when no ambient current is present). This is called the random-phase model.

In case that an ambient current is present, it is assumed that it is uniform with respect to the vertical co-ordinate and the changes in the mean flow within a wave length are so small that they affect only negligibly the dispersion relation. The absolute radian frequency  $\omega$  then equals the sum of the relative radian frequency  $\sigma$  and the multiplication of the wave number and ambient current velocity vectors:

$$\omega = \sigma + \vec{k} \cdot \vec{u}_c \quad (2.60)$$

which is the usual Doppler shift with  $\vec{u}_c$  the current velocity and  $\vec{k}$  the wave number respectively. For linear waves, the relative frequency is given by

$$\sigma^2 = gk \tanh(kd) \quad (2.61)$$

where  $g$  is the acceleration of gravity,  $k$  is the wave number and  $d$  is the water depth. The presence of ambient currents may change the amplitude, frequency and direction of an incoming wave.

In the field of ocean wave theory, it is conventional to define a spectrum  $E(f)$  as:

$$E(f) = 2\tilde{E}(f) \quad \text{for } f \geq 0 \quad \text{and} \quad E(f) = 0 \quad \text{for } f < 0 \quad (2.62)$$

where  $\tilde{E}(f)$  is the variance density spectrum, which is the Fourier transform of the auto-covariance function of the sea surface elevation, (Holthuijsen, 2007):

$$\tilde{E}(f) = \int_0^{+\infty} C(\tau) e^{-2\pi i f \tau} d\tau$$

with

$$C(\tau) = \langle \eta(t)\eta(t + \tau) \rangle \quad (2.63)$$

where  $C(\tau)$  is auto-covariance function,  $\langle \rangle$  represents mathematical expectation of random variable and  $\eta(t), \eta(t + \tau)$  represent two random processes of sea surface elevation,  $\tau$  represents the time lag. As a result  $\tilde{E}(f)$  can be determined from a time series measurement in a single point.

The description of water waves through the defined variance density spectrum  $E(f)$  is called spectral description of water waves. It has been proved that the variance of the sea surface elevation is given by

$$\langle \eta^2 \rangle = C(0) = \int_0^{+\infty} E(f)df \quad (2.64)$$

which indicates that the spectrum distributes the variance over frequencies.  $E(f)$  should therefore be interpreted as a variance density. The dimensions of  $E(f)$  are  $m^2/Hz$  if the elevation is given in m and the frequencies in Hz. The variance  $\langle \eta^2 \rangle$  is equal to the total energy  $E_{tot}$  of the waves per unit surface area if multiplied with a properly chosen coefficient:

$$E_{tot} = \frac{1}{2}\rho_w g \langle \eta^2 \rangle \quad (2.65)$$

The energy density as a function of frequency and direction is denoted as  $E(f, \theta)$ . This spectrum distributes the wave energy over frequencies and directions. As the total energy density at a frequency  $f$  is distributed in the direction  $\theta$  as  $E(f, \theta)$ , where the angle  $\theta = (k_{x1}, k_{x2})$  with  $k_{x1} = \sin \theta$  and  $k_{x2} = \cos \theta$  it follows that the frequency of energy density spectrum without directional information :

$$E(f) = \int_0^{2\pi} E(f, \theta)d\theta \quad (2.66)$$

Based on the energy density spectrum, the integral wave parameters  $m_n$  can be obtained. These parameters can be expressed in terms of the so-called n -th moment of the energy density spectrum:

$$m_n = \int_0^{\infty} f^n E(f)df \quad (2.67)$$

The zeroth moment is equal to the variance :

$$m_0 = \int_0^{\infty} E(f)df = \langle \eta^2 \rangle \quad (2.68)$$

Thus, the variance of the sea surface elevation is given by  $m_0 = \langle \eta^2 \rangle$ .

The knowledge of the wave spectrum, for linear waves, allows the reconstruction of the full probability structure of the sea surface. Thus, the significant wave height:

$$H_s = 4m_0^{\frac{1}{2}} \quad (2.69)$$

where  $m_0^{\frac{1}{2}}$  plays the role of characteristic length scale.

Since the spectrum can be measured, the significant wave height can be determined by integration of the observed wave spectrum.

Some wave periods:

$$T_{m01} = \frac{m_0}{m_1}, \quad T_{m02} = \sqrt{\frac{m_0}{m_1}}, \quad T_{m-10} = \frac{m_{-1}}{m_0} \quad (2.70)$$

In SWAN, the energy density spectrum  $E(\sigma, \theta)$  is generally used. On a larger scale the spectral energy density function  $E(\sigma, \theta)$  becomes a function of space and time and wave dynamics should be considered to determine the evolution of the spectrum in space and time. For brevity, the notation  $E(\sigma, \theta)$  will still be used.

### 2.3.3 Propagation in an inhomogeneous medium

In the case of an inhomogeneous medium (varying depth and varying currents) it is possible to derive a relatively simple expression for the time evolution of  $\alpha$ :

$$\partial_t N + \nabla_x [\nu_D N] = 0, \quad (2.71)$$

with

$$N(x, t) = \frac{2|\alpha(x, t)|^2}{\sigma}$$

and

$$\nu_D = \nabla_k \Omega = U + c_g = \nabla_k \sigma(k(x, t)),$$

where the subscript  $k$  now denotes differentiation with respect to wave number. The equation (2.71) has the general form of a conservation law, in which the local rate of change of a density is determined by a flux of that density. It implies that the integral over all space of  $N$  is conserved in time.

Willebrand (1975) noted that the conservation of wave action, (1.63), holds for every wave component separately:

$$\frac{\partial}{\partial t} N_n + \nabla_x \cdot [\nabla_k \omega_n N_n] = 0, \quad N_n = 2 \frac{|\alpha_n|^2}{\sigma_n} \quad (2.72)$$

and in addition,

$$\omega_n(x, t) = \Omega(k_n), \quad \Omega(k) = \sigma(k) + k \cdot U, \quad (2.73)$$

$$\frac{\partial}{\partial t} k_n + \nabla_x \omega_n = 0. \quad (2.74)$$

where wave action density defined as  $N_n(x, t) = \frac{F_n(x, t)}{\sigma_n}$ . Moreover, in a continuous form the density of  $k$ -modes is a function of time and this leads to an extra term involving  $\nabla_x \Omega$  in the equation for  $N(k, x, t)$ :

$$\frac{\partial N(k, x, t)}{\partial t} + (\nabla_k \Omega) \cdot \nabla_x N(k, x, t) - (\nabla_x \Omega) \cdot \nabla_k N(k, x, t) = 0. \quad (2.75)$$

Explicitly, in terms of the wave spectrum  $F$ ,  $N(k, x, t) = \frac{F(k, x, t)}{\sigma(k)}$ , we have :

$$\left\{ \frac{\partial}{\partial t} + (\nabla_k \Omega) \cdot \nabla_x - (\nabla_x \Omega) \cdot \nabla_k \right\} \left( \frac{F(k, x, t)}{\sigma} \right) = 0. \quad (2.76)$$

Another useful form for this equation is obtained by using the trivial identity :

$$\nabla_x \cdot (\nabla_k \Omega) - \nabla_k \cdot (\nabla_x \Omega) = 0. \quad (2.77)$$

This leads to the 'flux form'

$$\frac{\partial}{\partial t} \left( \frac{F}{\sigma} \right) + \nabla_x \cdot \left[ (c_g + U) \left( \frac{F}{\sigma} \right) \right] - \nabla_k \cdot \left[ \nabla_x \Omega \left( \frac{F}{\sigma} \right) \right] = 0. \quad (2.78)$$

This equation has the form of a conservation law. It also holds in other coordinates, for example in terms of  $\omega, \theta$ . In particular, it implies conservation of the total wave action defined in (1.160).

The **action balance equation** is now obtained from (equations (1.173) and (1.185)). The general result for the evolution of the wave action density  $\frac{F(k, x, t)}{\sigma(k, x)}$  reads :

$$\left\{ \frac{\partial}{\partial t} + (c_g + U) \cdot \frac{\partial}{\partial x} - (\nabla_x \Omega) \cdot \frac{\partial}{\partial k} \right\} \left( \frac{F}{\sigma} \right) = \sum_{\ell} S'_{\ell}(F; u), \quad (2.79)$$

where the summation is over the different perturbations, we define  $S' = \frac{S}{\sigma}$  and  $u$  refers to 'environmental parameters', such as the surface wind speed and direction. The group velocity  $c_g$  the group velocity,  $U$  is the surface current and  $\Omega = \Omega(k) = \sigma(k) + k \cdot U$ . The equation describes the evolution of the wave variance spectrum  $F(k, x, t)$ , which characterizes the statistical properties of the sea surface. The left hand side describes propagation through a nonhomogeneous medium (currents, variable depth), which conserves total wave action as an adiabatic invariant. The right hand side consists of source terms describing wind input ( $S_{in}$ ), sinks (whitecapping dissipation  $S_{ds}$  + bottom terms) and a nonlinear interaction term  $S_{nl}$ .

Equation (2.79) is also known as the radiative transfer equation, the transport equation or the kinetic equation. The name Boltzmann equation is used when one considers the sole effect of four wave interactions. In that case the equation describes conservative interactions ('elastic collisions') between wave packets and is analogous to the equation describing the distribution of momentum over the molecules in a gas.

In deep water, without currents, (2.79) reduces to the simpler form

$$\left\{ \frac{\partial}{\partial t} + c_g \cdot \frac{\partial}{\partial x} \right\} F(k, x, t) = \sum_{\ell} S_{\ell}(F; u) = S_{in} + S_{nl} + S_{ds} \quad (2.80)$$

or equivalently

$$\frac{DF}{Dt} = S_{in} + S_{nl} + S_{ds}, \quad (2.81)$$

where  $\frac{D}{Dt}$  denotes differentiation when moving with the group velocity. In this form the equation is also known as the **energy balance equation**, since F is directly proportional to the energy spectrum.

### 2.3.4 Action and Energy balance equation

The main goal of the SWAN is to solve the spectral action balance equation without any *priori* restrictions on the spectrum for the evolution of wave growth. This equation represents the effects of spatial propagation, refraction, shoaling, generation, dissipation and nonlinear wave-wave interactions.

#### Action balance equation

Related wave prediction models are typically based in the energy balance equation in terms of absolute radian frequency  $\omega$  and density energy  $E(\omega, \theta)$ . However, in the case that ambient currents are present, the energy density  $E(\omega, \theta)$  is written in terms of the relative frequency  $E(\sigma, \theta)$ . On the other hand, the SWAN model is based on the spectral action balance equation in terms of relative radian frequency  $\sigma$  because unlike these other models SWAN accounts for wave-current interactions. The action density N is the contribution of waves in a certain direction and with a certain frequency to the total wave action. Usually, wave models determine the evolution of action density  $N(\vec{x}, t; \sigma, \theta)$  which is a function of space  $\vec{x}$  and time t (on a scale large compared with wave length and period) and of spectral coordinates (wave frequency and direction) and is defined as  $N(\sigma, \theta) = \frac{E(\sigma, \theta)}{\sigma}$ . In contrast to wave energy, wave action is conserved in the presence of currents (Whitham, 1974 ;Svendsen, 2006). Wave action is said to be adiabatic invariant. It assumed that the ambient current is uniform with respect to the vertical coordinate and is denoted as  $\vec{U}$ .

The evolution of the action density N at a single point in space ( $\vec{x}; \sigma, \theta$ ) and time t is governed by the action balance equation, which reads as (e.g., Mei, 1983; Komen et al., 1994):

$$\frac{\partial N(\vec{x}, t; \sigma, \theta)}{\partial t} + \underbrace{\nabla_{\vec{x}} \cdot [(\vec{c}_g + \vec{U})N(\vec{x}, t; \sigma, \theta)]}_1 + \underbrace{\frac{\partial c_{\sigma} N(\vec{x}, t; \sigma, \theta)}{\partial \sigma}}_2 + \underbrace{\frac{\partial c_{\theta} N(\vec{x}, t; \sigma, \theta)}{\partial \theta}}_3 = \frac{S_{tot}}{\sigma} \quad (2.82)$$

The left-hand side is the kinematic part of this equation. The term 1 denotes the propagation of wave energy in two-dimensional geographical  $\vec{x}$ -space, including wave shoaling, with the group velocity  $\vec{c}_g = \frac{\partial \sigma}{\partial \vec{k}}$  following from the dispersion

relation  $\sigma^2 = g|\vec{k}| \tanh(|\vec{k}|d)$  where  $\vec{k}$  is the wave number vector and  $d$  the water depth. The term 2 represents the effect of shifting of the radian frequency due to variations in depth and mean currents. The term 3 represents depth-induced and current-induced refraction. The quantities  $c_\sigma$  and  $c_\theta$  are the propagation velocities in spectral space  $(\sigma, \theta)$ . The right-hand side contains  $S_{tot}$ , which is the source or sink term that represents all physical process which generate, dissipate, or redistribute wave energy. They are defined for energy density  $E(\sigma, \theta)$ .

Equation(2.82) can be recasted in Cartesian or spherical co-ordinates. We use Cartesian co-ordinates to express the spectral action balance equation for small scale applications, as given by:

$$\begin{aligned} \frac{\partial N(x, y, t; \sigma, \theta)}{\partial t} + \underbrace{\frac{\partial c_x N(x, y, t; \sigma, \theta)}{\partial x} + \frac{\partial c_y N(x, y, t; \sigma, \theta)}{\partial y}}_1 + \\ \underbrace{\frac{\partial c_\sigma N(x, y, t; \sigma, \theta)}{\partial \sigma}}_2 + \underbrace{\frac{\partial c_\theta N(x, y, t; \sigma, \theta)}{\partial \theta}}_3 = \frac{S_{tot}(x, y, t; \sigma, \theta)}{\sigma} \end{aligned} \quad (2.83)$$

where  $c_x = c_{g,x} + U_x$ ,  $c_y = c_{g,y} + U_y$ . Moreover, the term 1 is the shoaling (depth), the term 2 is the frequency shift (current) and the term 3 is the refraction (depth, current) and diffraction (depth, obstacles).

When an ambient current is absent, equation(2.82) simplifies to the aforementioned energy balance equation:

$$\frac{\partial E(x, y, t; \omega, \theta)}{\partial t} + \frac{\partial c_x E(x, y, t; \omega, \theta)}{\partial x} + \frac{\partial c_y E(x, y, t; \omega, \theta)}{\partial y} + \frac{\partial c_\theta E(x, y, t; \omega, \theta)}{\partial \theta} = S(x, y, t; \omega, \theta) \quad (2.84)$$

where  $c_x = c_{g,x} + U_x$ ,  $c_y = c_{g,y} + U_y$  and  $\omega$  is absolute radian frequency,  $E(\omega, \theta)$  is the energy density spectrum and  $S(\omega, \theta)$  is the source term as described above.

For large-scale computations such as applications with oceanic waters or at shelf sea, SWAN offers the spectral action balance equation formulated in terms of spherical coordinates:

$$\begin{aligned} \frac{\partial \tilde{N}(\lambda, \varphi; \sigma, \theta)}{\partial t} + \frac{\partial c_\lambda \tilde{N}(\lambda, \varphi; \sigma, \theta)}{\partial \lambda} + \frac{\partial c_\varphi \tilde{N}(\lambda, \varphi; \sigma, \theta)}{\partial \varphi} + \\ \frac{\partial c_\sigma \tilde{N}(\lambda, \varphi; \sigma, \theta)}{\partial \sigma} + \frac{\partial c_\theta \tilde{N}(\lambda, \varphi; \sigma, \theta)}{\partial \theta} = \frac{S_{tot}}{\sigma} \end{aligned} \quad (2.85)$$

where action density  $\tilde{N}$  is with respect to longitude  $\lambda$  and latitude  $\varphi$ . Note that  $\theta$  is the wave direction taken counterclockwise from geographic East. The propagation velocities are reformulated as follows. On a sphere, we have

$$dx = R \cos \varphi d\lambda \quad (2.86)$$

$$dy = R d\varphi$$

with  $R$  the radius of the earth. The propagation velocities in geographic space are then given by

$$\frac{d\lambda}{dt} = c_\lambda = \frac{1}{R \cos \varphi} \left[ \frac{1}{2} \left( 1 + \frac{2|\vec{k}|d}{\sinh(2|\vec{k}|d)} \right) \frac{\sigma|\vec{k}| \cos \theta}{|\vec{k}|^2} + u_\lambda \right] \quad (2.87)$$

$$\frac{d\varphi}{dt} = c_\varphi = \frac{1}{R} \left[ \frac{1}{2} \left( 1 + \frac{2|\vec{k}|d}{\sinh(2|\vec{k}|d)} \right) \frac{\sigma|\vec{k}| \sin \theta}{|\vec{k}|^2} + u_\varphi \right]$$

with  $u_\lambda$  and  $u_\varphi$  the ambient currents in longitude and latitude direction, respectively. The propagation velocity in  $\sigma$ -space remain unchanged. To rewrite the propagation velocity  $\tilde{c}_\theta$  in terms of spherical co-ordinates, we use the so-called Clairaut's equation that states that on any geodesic, the following expression holds:

$$R \cos \varphi \cos \theta = \text{constant} \quad (2.88)$$

Differentiation of Eq. (2.88) with respect to a space co-ordinate  $s$  in wave direction gives

$$-R \sin \varphi \cos \theta \frac{d\varphi}{ds} - R \cos \varphi \sin \theta \frac{d\theta}{ds} = 0 \quad (2.89)$$

Since,  $dy = ds \sin \theta$ , we have  $\frac{d\varphi}{ds} = \frac{\sin \theta}{R}$ . Substitution into Eq. (2.89) and using  $ds = (c_x \cos \theta + c_y \sin \theta) dt$  yields

$$\frac{d\theta}{dt} = -\frac{c_x \cos \theta + c_y \sin \theta}{R} \cos \theta \tan \varphi \quad (2.90)$$

This term (2.90) accounts for the change of propagation direction relative to true North when traveling along a great circle. This holds for deep water and without currents. Hence,

$$\tilde{c}_\theta = c_\theta - \frac{c_x \cos \theta + c_y \sin \theta}{R} \cos \theta \tan \varphi \quad (2.91)$$

In Eq.(2.86),  $\tilde{N}$  is related to the action density  $N$  in a local Cartesian frame  $(x, y)$  through  $\tilde{N} d\sigma d\theta d\varphi d\lambda = N d\sigma d\theta dx dy$ , or  $\tilde{N} = N R^2 \cos \varphi$ . Substitution into (2.86) yields:

$$\frac{\partial N}{\partial t} + \frac{\partial c_\lambda N}{\partial \lambda} + \cos^{-1} \frac{\partial c_\varphi \cos \varphi N}{\partial \varphi} + \frac{\partial c_\sigma N}{\partial \sigma} + \frac{\partial c_\theta N}{\partial \theta} = \frac{S_{tot}}{\sigma} \quad (2.92)$$

with longitude  $\lambda$  and latitude  $\varphi$ .

Using the proper expressions for the propagation speeds  $c_g$  and  $c_\theta$  and  $c_\sigma$  in the action balance equation, which are derived from the linear theory (Holthuijsen, 2007; Whitham, 1974; Mei, 1983) the effects of wave propagation (shoaling, refraction and frequency shifting ; diffraction is neglected here) are accounted for:

$$\frac{D\vec{x}}{dt} = (c_x, c_y) = \vec{c}_g + \vec{u} = \frac{1}{2} \left( 1 + \frac{2|k|d}{\sinh(2|k|d)} \right) \frac{\sigma \vec{k}}{|k|^2} + \vec{u} \quad (2.93)$$

$$\frac{D\sigma}{dt} = c_\sigma = \frac{\partial \sigma}{\partial d} \left( \frac{\partial d}{\partial t} + \vec{u} \cdot \nabla_{\vec{x}} d \right) - c_g \vec{k} \cdot \frac{\partial \vec{u}}{\partial s}$$

$$\frac{D\theta}{dt} = c_\theta = -\frac{1}{k} \left( \frac{\partial \sigma}{\partial d} \frac{\partial d}{\partial m} + \vec{k} \cdot \frac{\partial \vec{u}}{\partial m} \right)$$

where  $c_x, c_y$  are the propagation velocities of wave energy in spatial  $x, y$ -space,  $c_\sigma$  and  $c_\theta$  are the propagation velocities of wave energy in spectral space  $\sigma, \theta$ -space,  $d$  is water depth,  $s$  is the space coordinate in the wave propagation direction of  $\theta$  and  $m$  is a co-ordinate perpendicular to  $s$ . Also,  $\vec{k} = (k_x, k_y) = (|\vec{k}| \cos \theta, |\vec{k}| \sin \theta)$  and the current velocity  $\vec{u} = (u_x, u_y)$

Furthermore, the operator  $\frac{D}{dt}$  denotes the total derivative along a spatial path of energy propagation, and is defined as

$$\frac{D}{dt} = \frac{\partial}{\partial t} + (\vec{c}_g + \vec{u}) \cdot \nabla_{\vec{x}} \quad (2.94)$$

with the group velocity  $\vec{c}_g = \frac{\partial \sigma}{\partial \vec{k}}$  following from the dispersion relation  $\sigma^2 = g|\vec{k}| \tanh(|\vec{k}|d)$  where  $\vec{k}$  is the wave number vector and  $d$  the water depth.

The right-hand side of the equation (2.82) contains source terms, i.e. terms which model the generation and dissipation of wave energy. In contrast with the propagation terms most of the source terms are empirical in nature and contain empirical "constants". SWAN has default values for almost all of these constants; these values are mostly based on literature, and have been obtained by studying laboratory experiments or field observations. Due to the empirical nature of parts of the model a verification is needed for every new application of the model.

The total sum of source and sink terms  $S_{tot}$ , in  $3^d$  generation formulations are divided into six processes :

$$S_{tot} = S_{in}(\sigma, \theta) + S_{nl4}(\sigma, \theta) + S_{wcap}(\sigma, \theta) + S_{nl3}(\sigma, \theta) + S_{br}(\sigma, \theta) + S_{bot}(\sigma, \theta) \quad (2.95)$$

where

- $S_{in}$  wave growth by the wind
- $S_{nl4}$  nonlinear quadruplets wave-wave interactions
- $S_{nl3}$  nonlinear triads wave-wave interactions
- $S_{wcap}$  dissipation due to white-capping
- $S_{br}$  dissipation due to depth-induced wave breaking
- $S_{bot}$  dissipation due to bottom friction

For more details about the modeled processes and the numerical methods used in SWAN, the reader is referred to (Komen et al., 1994) and (Wave, User manual).

For a full wave-current interaction, the currents from Delft3D-FLOW are used in Delft3D-WAVE (current refraction). The procedure is known as the coupling of the two models. The interaction between waves and currents is implemented by running the wave model every  $N$  flow time steps. The wave module must run before the flow module. A communication file is created that contains the results of the wave simulation (rms wave height, peak period, wave direction, mass fluxes etc). The flow module can read then the wave results and include them in the flow simulation. The reason that the wave model is called more than once is that the computed wave model must be updated in order to account for the changed water depths and flow properties. At each call to the wave module, the latest bed and water elevations and current velocities are transferred from the flow module.

## 2.4 Boundary conditions

To get a well-posed mathematical problem with a unique solution, a set of initial and boundary conditions for water levels and horizontal velocities must be specified. The contour of the model domain consists of parts along land-water lines (coast lines) which are called closed boundaries and parts across the flow field which are called open boundaries. Closed boundaries are natural boundaries. The velocities normal to a closed boundary are set to zero. Open boundaries are always artificial "water-water" boundaries (Flow, User Manual).

### 2.4.1 Vertical boundary conditions

#### **Kinematic Boundary Conditions:**

In the  $\sigma$  coordinate system, the free surface ( $\sigma=0$ , or  $z=\zeta$ ) and the bottom ( $\sigma = -1$ , or  $z = -d$ ) are  $\sigma$ -coordinate surfaces. The impermeability of the surface and the bottom is taken into account by prescribing the following kinematic conditions:

$$\omega|_{\sigma=-1} = 0 \quad \text{and} \quad \omega|_{\sigma=0} = 0 \quad (2.96)$$

where  $\omega$  is the vertical velocity relative to the  $\sigma$ -plane.

#### **Bed Boundary Condition:**

At the seabed, the boundary conditions for the momentum equations are:

$$\frac{v_V}{H} \frac{\partial u}{\partial \sigma} \Big|_{\sigma=-1} = \frac{\tau_{bx}}{\rho_0} \quad (2.97)$$

$$\frac{v_V}{H} \frac{\partial v}{\partial \sigma} \Big|_{\sigma=-1} = \frac{\tau_{by}}{\rho_0} \quad (2.98)$$

where  $\tau_{bx}$  and  $\tau_{by}$  are the components of the bed stress in x and y direction, respectively, that include the effects of wave - current interaction. Their formulation for the combination of flow and wave will be discussed later.

The bed shear stress in 3D is related to the current just above the bed:

$$\vec{\tau}_{b3D} = \frac{g\rho_0\vec{u}_b |\vec{u}_b|}{C_{3D}^2} \quad (2.99)$$

where  $|\vec{u}_b|$  is the magnitude of the horizontal velocity in the first layer just above the bed and  $C_{3D}$  is the Chezy coefficient (Delft3D - Flow, User Manual(2014)).

### Surface Boundary Condition:

At the free surface the boundary conditions for the momentum equations are:

$$\frac{v_V}{H} \frac{\partial u}{\partial \sigma} \Big|_{\sigma=0} = \frac{|\vec{\tau}_s|}{\rho_0} \cos(\theta) \quad (2.100)$$

$$\frac{v_V}{H} \frac{\partial v}{\partial \sigma} \Big|_{\sigma=0} = \frac{|\vec{\tau}_s|}{\rho_0} \sin(\theta) \quad (2.101)$$

where  $\theta$  is the angle between the wind stress vector and the local direction of the grid line y is constant. Without wind, the stress at the surface is zero. The magnitude of the wind shear - stress is defined as:

$$|\vec{\tau}_s| = \rho_0 \vec{u}_{*s} |\vec{u}_{*s}| \quad (2.102)$$

where  $u_{*s}$  is the friction velocity at the free surface and it can be determined by the following widely used quadratic expression:

$$|\vec{\tau}_s| = \rho_\alpha C_d U_{10}^2 \quad (2.103)$$

where:

$\rho_\alpha$  the air density

$U_{10}$  the wind speed 10 meter above the free surface

$C_d$  the wind drag coefficient, depending on  $U_{10}$

### 2.4.2 Open boundary conditions

Open boundaries are artificial, water-water boundaries. They are situated as far away as possible from the area of interest and they are introduced to obtain a limited computational area and so to reduce the computational effort.

In general, the boundary conditions are specified in a limited number of boundary points. Linear interpolation is used to generate the boundary conditions at the intermediate points along the boundary. This interpolation can generate physical

unrealistic flows in the region close to the open boundary. The boundary conditions should allow these disturbances to propagate out of the area. Alternatively, the number of points where the boundary condition is specified should be extended.

For the needs of this study, we follow (Roelvink et. al., 2004). According to this paper, one main problem is the specification of suitable boundary conditions at the open boundaries. This is due to a combination of processes acting on the model domain, resulting in the development of a certain water level or velocity in the cross - shore direction. For the boundary conditions to match this distribution the solution has to be known beforehand, otherwise boundary disturbances will develop.

In order to overcome this problem, (Roelvink et. al., 2004) suggest to let the model determine the correct solution at the boundaries by imposing the along-shore water level gradient (a so-called Neumann boundary condition) instead of a fixed water level or velocity. In this case, it is assumed to be zero. Neumann boundaries can only be applied on cross-shore boundaries in combination with a water level boundary,  $\zeta = F_\zeta(t)$ , which is needed to make the solution of the mathematical boundary value problem well- posed.

To reduce the reflections at the open boundary (Verboom and Slob, 1984; Verboom and Segal, 1986) derived a so-called zero and first order weakly reflecting boundary condition based on the work of Engquist and Majda (1977, 1979). Assuming zero flow along the boundary, the zero order boundary condition may also be obtained using the so-called Riemann invariants for the linearised 1D equation normal to the open boundary:

$$R = U \pm 2\sqrt{gH} \quad (2.104)$$

where  $U$  is the velocity in normal direction,  $g$  the acceleration due to gravity and  $H$  the total water level.

The two Riemann invariants are two waves moving in opposite direction with propagation speed  $R = U \pm \sqrt{gH}$ . The sign is dependent on the direction of propagation. At the open boundary, the incoming wave should be specified. We restrict ourselves to the positive sign (left boundary). The linearised Riemann invariant is given by:

$$U + 2\sqrt{gH} = U + 2\sqrt{g(d + \zeta)} \approx U + 2\sqrt{gd} + \zeta\sqrt{\frac{g}{d}}, \quad \frac{|\zeta|}{d} \ll 1. \quad (2.105)$$

where  $d$  is the local depth,  $\zeta$  is the free surface elevation and the sign is depend on the  $U$  direction perpendicular to our boundary. The boundary condition which should be specified by us is  $f(t) = U + \zeta\sqrt{\frac{g}{d}}$ , where the term  $2\sqrt{gd}$  is computed from the known depth-field and added in the computational part. It is assumed that the reference plane is chosen such that the mean water level is zero.

In the computational part, we distinguish the following type of boundary conditions in this study (for simplicity only a description for the U-direction is given):

- Water level:  $\zeta = F_\zeta(t) + \delta_{atm}$ ,
- Velocity (in normal direction):  $U = F_U(t)$ ,
- Riemann invariant  $U \pm \zeta \sqrt{\frac{g}{d}} = F_R(t)$ .

where  $\delta_{atm}$  is the pressure and it will be prescribed bellow.

On water level boundaries, an input signal is prescribed that is consistent with some average pressure. Usually the signal corresponds to Mean Sea Level. One actually wants to prescribe an input signal corresponding to the local pressure prescribed by the space varying meteo input. To this end, it is possible to specify an average pressure ( $p_{average}$ ) which should correspond to your input signal on the open boundaries, which is then used to determine local pressure gradients that need to be applied along the open boundaries to obtain an input signal that is consistent with the local atmospheric pressure. The pressure must be specified in  $N/m^2$ .

$$\delta_{atm} = \frac{p_{average} - p_{atm}}{\rho g} \quad (2.106)$$

where :

$p_{average}$  average pressure

$p_{atm}$  the local atmospheric pressure, given by the meteo module

$\rho$  density of water

$g$  acceleration due to gravity

On Riemann boundaries can be used the same correction and is calculates as :

$$F_R(t) = F_R(t) \pm \delta_{atm} \sqrt{\frac{g}{d}} \quad (2.107)$$

with  $d$  the local water depth and the sign depends on the orientation of the open boundary related to the grid.

For the velocity and Riemann type of boundary condition, the flow is assumed to be perpendicular to the open boundary. Substitution of the Riemann boundary condition in the 1D linearised continuity equation leads to the well-known radiation boundary condition.

Stelling (1984) added the time-derivative of the Riemann invariant to the water level and velocity boundary conditions, to make the boundaries less reflective for

disturbances with the eigen frequency of the model area. This reduces the spin-up time of a model from a cold start:

$$\text{Water level boundary : } \zeta + \alpha \frac{\partial}{\partial t} \left\{ U \pm 2\sqrt{gH} \right\} = F_\zeta(t) \quad (2.108)$$

$$\text{Velocity boundary : } U + \alpha \frac{\partial}{\partial t} \left\{ U \pm 2\sqrt{gH} \right\} = F_U(t) \quad (2.109)$$

The reflection coefficient  $\alpha$  should be chosen sufficiently large to damp the short waves introduced at the start of the simulation. The following values are advised:

$$\text{Water level boundary : } \alpha = T_d \sqrt{\frac{H}{g}} \quad , [s^2] \quad (2.110)$$

$$\text{Velocity boundary : } \alpha = T_d \quad , [s] \quad (2.111)$$

where  $T_d$  is the time it takes for a free surface wave to travel from the left boundary to the right boundary of the model area. In ocean and sea models, the period  $T_d$  is of the same order as the period of the tidal forcing. In that case  $\alpha$  must be set to zero, otherwise effectively the amplitude of one of the components in the boundary condition is reduced. These values can be derived with Fourier analysis for the 1D linear long wave equation without advection by substituting a wave with period  $T_d$ .

For the velocity type of boundary condition, the flow is assumed to be perpendicular to the open boundary. In 3D models we can prescribe 3 profiles in the vertical:

- a uniform profile
- a logarithmic profile
- a so-called 3D profile

A 3D profile means that the velocity at each  $\sigma$ -layer is specified as any of forcing types, i.e. as astronomic or time-series components.

## Astronomic boundary conditions

We can specify the boundary conditions in terms of astronomical components. The observed tidal motion can be described in terms of a series of simple harmonic constituent motions, each with its own characteristic frequency  $\omega$  (angular velocity). The amplitudes  $A$  and phases  $G$  of the constituents vary with the positions where the tide is observed.

The general formula for the astronomical tide is:

$$H(t) = A_0 + \sum_{i=1}^k A_i F_i \cos(\omega_i t + (V_0 + u)_i - G_i) \quad (2.112)$$

where:

$H(t)$	water level at time $t$
$A_0$	mean water level over a certain period
$k$	number of relevant constituents
$i$	index of a constituent
$A_i$	local tidal amplitude of a constituent
$F_i$	nodal amplitude factor
$\omega_i$	angular velocity
$(V_0 + u)_i$	astronomical argument
$G_i$	improved kappa number

$F_i$  and  $(V_0 + u)_i$  are time-dependent factors which, together with  $\omega$ , can easily be calculated and are generally tabulated in the various tidal year books.  $V_0$  is the phase correction factor which relates the local time frame of the observations to an internationally agreed celestial time frame.  $V_0$  is frequency dependent.  $F_i$  and  $u_i$  are slowly varying amplitude and phase corrections and are also frequency dependent. For most frequencies they have a cyclic period of 18.6 years.  $A_0$ ,  $A_i$  and  $G_i$  are position-dependent: they represent the local character of the tide.

### 2.4.3 Closed boundary conditions

A closed boundary is situated at the transition between land and water. At a closed boundary, two boundary conditions have to be prescribed. One boundary condition has to do with the flow normal to the boundary and the other one with the shear-stress along the boundary. The boundary condition considered for flow normal to the boundary is that there is no flow through the boundary. For the shear stress along the boundary a zero tangential shear-stress (free slip) has been prescribed.

## 2.5 Numerical aspects

The numerical method of Delft3D-FLOW is based on finite differences. An alternating direction implicit (ADI) method is used to solve the continuity and horizontal momentum equations (Leendertse, 1987). Stelling (1984) extended the ADI method of Leendertse with a special approach for the horizontal advection terms, known as the "cyclic method" (Stelling and Leendertse, 1991). The transport equation is formulated in a conservative form (finite - volume approximation) and is solved using the so-called "cyclic method" of Stelling and Leendertse (1991), including the algorithm of Stelling and Van Kester (1994) for the approximation of the horizontal diffusion along z-planes in a  $\sigma$ -coordinate framework. The reader is referred to the Delft3d-FLOW, User Manual (2014) for more details about the

numerical methods applied in the Delft3d model.

The numerical grid transformation is implicitly known by the mapping of the coordinates of the grid vertices from the physical to the computational space. The  $\sqrt{G_{\xi\xi}}$  and  $\sqrt{G_{\eta\eta}}$  geometrical quantities introduced in the transformed equations.

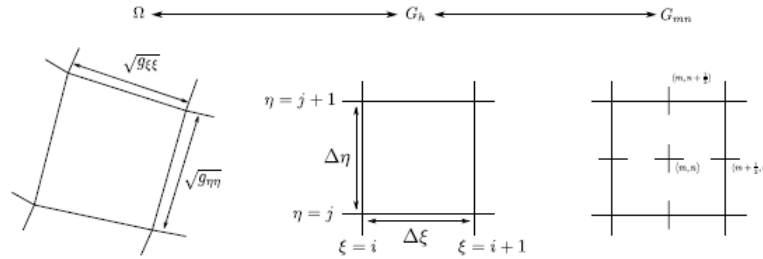


Figure 2.5: Mapping of physical space to computational space

### Staggered grid

The primitive variables water level and velocity ( $u$ ,  $v$ ,  $w$ ) describe the flow. To discretise the 3D shallow water equations, the variables are arranged in a special way on the grid, see Figure 5. The pattern is called a staggered grid. This particular arrangement of the variables is called the Arakawa C-grid. The water level points (pressure points) are defined in the center of a (continuity) cell. The velocity components are perpendicular to the grid cell faces where they are situated. Staggered grids have several advantages such as:

- Boundary conditions can be implemented in a rather simple way.
- It is possible to use a smaller number of discrete state variables in comparison with discretizations on non-staggered grids, to obtain the same accuracy.
- Staggered grids for shallow water solvers prevent spatial oscillations in the water levels; see e.g. Stelling (1984).

The staggered grid applied in Delft3D is given in Figure 6 with the following legend:

**full lines** the numerical grid

**grey area** items with the same grid indices ( $m$ ;  $n$ )

+

water level, concentration of constituents, salinity, temperature

–

horizontal velocity component in  $u$ - and  $m$ - direction)

|

horizontal velocity component in  $v$ - and  $n$ - direction

•

depth below mean (still) water level (reference level)

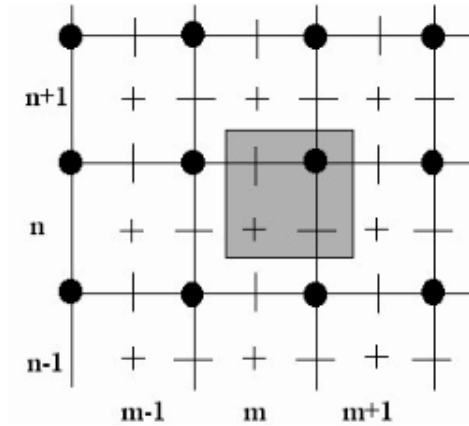


Figure 2.6: Staggered grid used in Delft3D-FLOW

An explicit time integration of the shallow water equations on a rectangular grid is subject to a time step condition based on the Courant Friedrichs Lewy (CFL) number for wave propagation:

$$CFL_{wave} = 2\Delta t \sqrt{gH} \sqrt{\frac{1}{\Delta x^2} + \frac{1}{\Delta y^2}} < 1 \quad (2.113)$$

where  $\Delta t$  is the time step,  $g$  is the acceleration of gravity,  $H$  is the total water depth and are the smallest grid spaces in  $\xi$ - and  $\eta$ -direction of the physical space.

# Chapter 3

## Data Analysis

### 3.1 About Copernicus

COPERNICUS, previously known as GMES (Global Monitoring for Environment and Security), is the European Programme for the establishment of a European capacity for Earth Observation and Monitoring.

COPERNICUS encompasses 3 components: SPACE , INSITU and SERVICES.

- **The Copernicus Space Component**

It includes 1. the ESAs Sentinels, which are currently being developed for the specific needs of the Copernicus programme and 2. the Contributing Missions, which are operated by national, European or international organisations and already provide a wealth of data for Copernicus services.

The European Space Agency (ESA) is responsible for the space component of the Copernicus programme. The European Organisation for the Exploitation of Meteorological Satellites (EUMETSAT) is fundamental to the operational remit of Copernicus on account of their unparalleled experience and proven capability as a provider of operational meteorological satellite data, products and services.

- **The Copernicus InSitu component**

Copernicus services rely on data from in situ monitoring networks (e.g. maps, ground based weather stations, ocean buoys and air quality monitoring networks) to provide robust integrated information and to calibrate and validate the data from satellites.

Surface moorings measure a wide variety of ocean sub-surface variables including Temperature, Salinity, Currents over long periods of time . These measures are widely used by MyOcean(Credit : Karlson/SMHI)

The in situ networks are managed by Members States and international bodies and make data available to the services by agreement.The European Environment Agency (EEA) is leading work for Copernicus under the FP7

GIS project to catalogue the in situ requirements of the Copernicus services, develop frameworks and pilot agreements to ensure access to all the relevant data in a timely and sustainable way.

- **The Copernicus Service component**

Copernicus services address six main thematic areas:

1. Land Monitoring
2. Emergency Management
3. Marine Monitoring
4. Atmosphere Monitoring
5. Security
6. Climate Change

These services have reached different degrees of maturity. Some are already operational (land monitoring and emergency management) while others are still in a pre-operational mode (atmosphere monitoring and marine monitoring), or in a development phase (climate change monitoring and services for security applications).

On November 11th, the European Commission and Mercator Ocean have signed an Agreement to implement and manage the Copernicus Marine Environment Monitoring Service. The latter is operational from early May 2015.

Today, the Copernicus Marine Service is provided on an operational mode by Mercator Ocean to more than 5000 subscribers worldwide.

## **3.2 Procedure of CMEMS**

Copernicus - Marine environment monitoring service, provides products and services for all marine applications. We use this platform to take ocean products about a specific region domain that we study. Firstly, we choose the region domain - Mediterranean Sea. Furthermore, we choose the parameters for our studying (current velocity) and the temporal coverage which is five days, from 16 January of 2019 to 21 January of 2019. In addition, we select the ocean product, in our case is the Mediterranean Sea Physics analysis and forecast. The physical component of the Mediterranean Forecasting System (Med-currents) is a coupled hydrodynamic-wave model implemented over the whole Mediterranean Basin. The model horizontal grid resolution is 1/24 (ca. 4 km) and has 141 unevenly spaced vertical levels. The hydrodynamics are supplied by the Nucleus for European Modelling of the Ocean (NEMO v3.6) while the wave component is provided by Wave Watch-III; the model solutions are corrected by a variational data assimilation scheme (3DVAR) of temperature and salinity vertical profiles and along track satellite Sea Level Anomaly observations. In the sequel, we choose the suitable data set,

specify the co-ordinates of the grid and choose the time-range and the number of layers of depth. Finally, we select the variables of the data-set that we study and download these information in a netcdf file.

### 3.3 R program and connection with open boundary conditions

We open our data from the netcdf file through the R programming language. We interpolate these data and create the format of time-series flow boundary conditions (.bct file). Firstly, we make a linear interpolation in depth and in longitude. Due to the fact that the grid of copernicus has bigger resolution from our grid.

Generally, for each open boundary segment with boundary data of type time-series the data is given in two related blocks:

1. A header block containing a number of compulsory and optional keywords accompanied by their values.
2. A data block containing the time dependent data.

We have a model with 31 open boundary sections with time-series as boundary conditions.

All the boundary sections concern a Riemann boundary for which the boundary condition is given at 25 time breakpoints, from 1051200 to 1052640 minutes after the Reference Date. The vertical profile is 3d-profile, the interpolation method linear, the time-series is assumed to be non-equidistant and the time is given in minutes.

### 3.4 Procedure of Delft Dashboard

Delft Dashboard is a Matlab based graphical user interface, which can run as a standalone executable or within Matlab. It is designed to support modellers in setting up new or upgrading and running existing models. A large number of coupled toolboxes allow Delft Dashboard for fast and easy model input generation. It allows an initial model to be set-up in a matter of minutes for every location in the world, which previously used to take days or weeks. The interface is coupled to the Delft3D modeling suite, which allows carrying out the hydrodynamics, the waves, the morphodynamics and the water quality computations. Besides the toolboxes, to set-up a standard Delft3D computation, additional toolboxes are implemented to carry out advanced tidal analysis, simulate wind speed and barotropic pressure changes generated by a tropical cyclone, and simulate the generation and propagation of a tsunami. Using the Delft Dashboard toolbox, the user can easily define the modelling area of interest. The user may perform all actions needed to run the models, as the definition of the computational grid boundaries, the determination of the grid cell size, the import of bathymetric data of the area, the designation of boundaries and boundary types on the grid and finally the insertion of boundary

conditions.

As described before, the Delft Dashboard graphical user interface is a useful tool to determine the characteristics of the modelling domain in the area of interest. In order to create the computational grid of each Observatory, a first approach was performed using a numerical grid based on a ratio of 1:4.17 from the Marine Copernicus Grid, resulting in a downscale to 1/100 degree ( $\sim 1,110$  m horizontal resolution). The vertical discretization of each Observatory is based on CMEMS "MEDITERRANEAN SEA PHYSICS ANALYSIS AND FORECAST" discretization and it differs in each Observatory.

The methodology of creation of an initial hydrodynamic model for every single Observatory follows the same typical steps.

1. Computational Grid Boundaries and Grid Cell Size Definition
2. Extraction and interpolation of bathymetric data
3. Extraction and interpolation of tidal boundary conditions
4. Creation of boundary conditions for the model

Initially, through the Delft Dashboard graphical user interface, the grid outline and the cell size of the horizontal resolution of the modelling domain of each Observatory was defined. The toolkit automatically creates the rectangular grid of the modelling domain within the boundaries specified in the toolkit with the fixation of the grid cells.

Afterwards, in order to finalize the grid determination, bathymetric data are attributed to the generated rectangular grid. As the present configuration, described in this document is only for testing proposes, and due to lack of local bathymetry data, the GEBCO 08 and the EMODNET bathymetry datasets were used in each Observatory. GEBCO's aim is to provide the most authoritative publicly-available bathymetry of the world's oceans. It operates under the joint auspices of the International Hydrographic Organization (IHO) and the Intergovernmental Oceanographic Commission (IOC) (of UNESCO). Moreover, EMODnet Bathymetry aims to provide a single access point to bathymetric products, Digital Terrain Models (DTM) and data (survey data sets and composite DTM) collected and managed by an increasing number of organisation from government and research scattered over Europe. Within Delft Dashboard, the bathymetry datasets were initially imported to the modelling domain and afterwards a spatial interpolation from the original grid to the model grid was carried out by linear interpolation.

As soon as the computational grid was generated, the Open Boundaries of the pilot Observatory may be defined. Delft Dashboard generates these open boundaries with an automated toolbox. To allow the hydrodynamic model, described in the present document, to have common boundaries with the CMEMS operational

hydrodynamic model and as the ratio of the numerical grid to CMEMS computational grid is  $\sim 1:4.17$ , approximately 4 cells per section were used to divide the open boundary cells to sections. Then at each section, a Riemann open boundary condition was applied using data on astronomical forcing derived from a global tidal model, TPXO 7.2. Delft Dashboard, through the 'Tide Database' toolbox, automatically creates open boundary conditions at each section of the open boundary cells, by retrieving tidal information (amplitude and phases) from the TPXO 7.2 Global Tidal Solution. As Riemann boundaries are depth-dependent a minimum depth of the open boundary cell has to be specified. It is recommended by Delft3D manual to set this value to at least 2 times the expected tide range. When setting up the initial models it was chosen to set this minimum depth to 5 m.

The scenario of our study in the hydrodynamic model Delft3D-flow concerns the Thracian Sea. The Reference date was the 16-01-2017, while the time period of the simulation was during five days, from 16-01-2019 00:00:00 to 21-01-2019 00:00:00, with time step 2 minutes. At first, we create a grid file through the Dashboard platform. It includes the co-ordinates of the orthogonal curvilinear grid at the depth points, with longitude  $x_{min}=24.2735$  and latitude  $y_{min}=40.2718$ . In this way, the computational grid enclosure file is created at the same time which contains the pairs of M and N indices (Mmax=313 and Nmax=73) representing the grid co-ordinates where a line segment of the computational grid enclosure (polygon) changes direction. This file is strongly related to the curvilinear grid file. In addition, we construct a bathymetry file using the data set Aegean Sea-Levantine Sea, which contains the bathymetry in the model area, represented by depth values (in metres) for all grid points. The co-ordinate system is spherical and this scenario contains 10 layers of depth because we have a 3D computation, in which every layer has different thickness in the form of percentage. The total percentage of thickness is 100. The type of our vertical grid is Z-grid, thus the layer thickness is fixed and the number of active layers varies with the depth. The layer thickness at the top is however determined by the actual water level and at the bottom by the local topography. For a Z-model the thickness of a layer is defined as a percentage of the initial water depth and the first layer refers to the bottom layer. Moreover, we construct a Water level open boundary file with 31 South open boundary sections and astronomic type of data and initial water level 0 metres, which contains the location and description of open boundaries. The tidal model that we use to generate these boundaries is TPXO 7.2 Global Inverse Tide Model. TPXO is a series of fully-global models of ocean tides, which best-fits, in a least-squares sense, the Laplace Tidal Equations and altimetry data. Each next model in TPXO series is based on updated bathymetry and assimilates more data compared to previous versions. The methods used to compute the model are described in details by Egbert, Bennett, and Foreman, 1994 and further by Egbert and Erofeeva, 2002. The tides are provided as complex amplitudes of earth-relative sea-surface elevation for eight primary (M2, S2, N2, K2, K1, O1, P1, Q1), two long period (Mf, Mm) and 3 non-linear (M4, MS4, MN4) harmonic constituents (plus 2N2 and S1 for TPXO9). Furthermore, we create the astronomic flow boundary conditions file, which contain the boundary conditions for open boundary sections

of type Astronomic in terms of amplitudes and phases for the astronomic components. All these files are generated in the platform of Delft Dashboard. Now, we use the FLOW-GUI to create Riemann open boundary with time-series forcing type and vertical profile per layer specified. Then, we upload the bct file that have been created through the R program.

# Chapter 4

## Test case and model setup

The Thracian Sea/North Aegean Observatory is located at the northern-most part of the Aegean Sea. It covers an area of  $\sim 12,100$  sq. km and has a volume of  $\sim 2,416$  cubic km. The area is directly affected by the Black Sea Water out flow from Dardanelles and three major rivers (Evros, Nestos and Strimon) which are located along the northern mainland coastline.

The modeling hydrodynamic system is based on a downscaling methodology, from CMEMS ( $1/24^\circ$ ) to a new grid with  $1/100^\circ$  ( $\sim 1.1$ km) for the region of Thracian Sea. The computational grid that was created is composed by  $313 \times 73$  cells in the horizontal and 10 Cartesian layers (in total 135,010 cells) that are based on CMEMS vertical discretization but follow a logarithmic increase in layer thickness with depth. This configuration following exactly the CMEMS discretization. The bathymetry data of the grid were retrieved through the Delft dashboard using the Aegean and Levantine dataset, which is part of EMODNET bathymetry data, and has a horizontal resolution of  $\sim 463$  m. In addition, the retrieved grid was interpolated spatially to fit the computational grid.

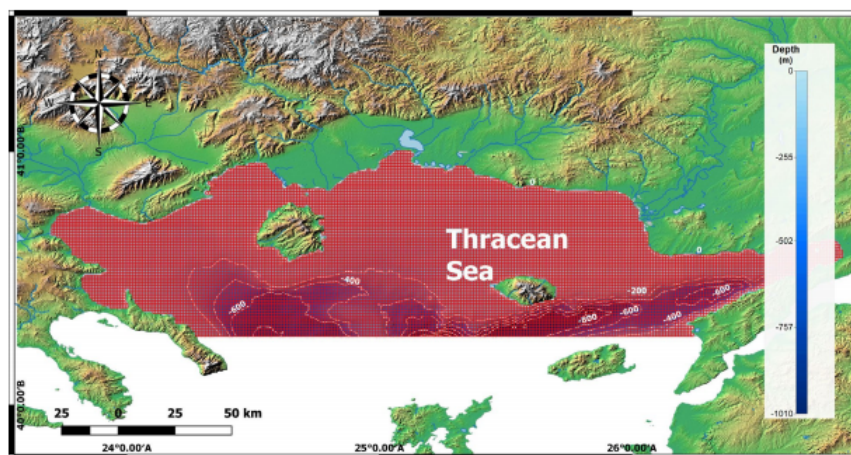


Figure 4.1: Computational grid of Thracian Sea

The grid's lower western origin coordinates are  $40.2718^\circ$  N,  $24.2735^\circ$  E and

has one open boundary located at the southern border line of the grid along the  $40.2718^\circ$  N latitude. Despite the fact that the initially designed grid was set so as the open boundary is located along the line connecting the southern part of Athos peninsula and the southern part of Gallipoli peninsula, this grid was moved northwards to avoid the direct effect of the Black Sea Water outflow from Dardanelles in the area. The length of the final open boundary is  $\sim 221$  km and fits well with 44 cells of the CMEMS computational grid for the Mediterranean Sea. Therefore, the open boundary cells are divided into sections, following the CMEMS grid (4 grid cells per section) in order to use data from the CMEMS hydrodynamic forecast run as boundary conditions. These boundary conditions are created by interpolating CMEMS grid data to the Observatory's computational grid for each section. The data that are downloaded from the CMEMS server are imported and stored into R data analysis program. As the Delft3D model will be run daily, a long time-series of the CMEMS downloaded parameters can be retrieved through the R program. The meteorological forcing of the hydrodynamic model is based on the import of data originating from the NOAA Global Forecast System (GFS). This system is a weather forecast model produced by the National Centers for Environmental Prediction (NCEP). Dozens of atmospheric and land-soil variables are available through this dataset, from temperatures, winds, and precipitation to soil moisture and atmospheric ozone concentration.

In addition, the computational grid is affected by the discharge of the three major rivers that outflow in the Thracian Sea. Discharge is the location where water and possibly constituents dissolved in the water are released into or subtracted from the model area. The discharge of these rivers was set to be constant in time for the purposes of this experimental run. Their values were based on the mean annual discharge data reported by research documents. The values for these discharges were: 1) for Nestos river  $30 \text{ m/s}^3$  2) for Strymon river  $80 \text{ m/s}^3$  3) for Evros river  $234 \text{ m/s}^3$ .

Moreover, we have two observation points, which are virtual points in the model area, where computational results, such as the current, the water level and/or the concentration of constituents are monitored as a function of time., in Thracian Sea. There is already one active hydro-meteorological station in Kavala port providing water temperature, salinity, and meteorological data and one oceanographic buoy located close to Kariani, at the western part of the Observatory, providing data for the validation of the Delft3D hydrodynamic model.

## 4.1 Swan Model set-up

For the operational wave modelling of the Thracian Sea a SWAN wave model was set up, using the Delft3D hydrodynamic model schematization as starting point. The rectangular computational grid covers the area between  $23.6935^\circ\text{E}$  to  $26.8335^\circ\text{E}$  in longitude and  $40.2719^\circ\text{N}$  -  $41.0119^\circ\text{N}$  in latitude, which is approximately 270 km in the EW direction » 80 km in the NS direction. The resolution of

the computational grid was set-up at  $1/100^\circ$  ( $\sim 1.1\text{km}$ ). Apart from a geographical domain, SWAN model also requires the definition of a spectral domain, covering wave frequencies and wave directions. The full directional circle is considered, divided in 45 directional bins of  $8^\circ$  each allowing the wave energy to propagate in any direction. Wave frequencies from 0.03 up to 1.0 Hz are included (wave periods 1 s – 33 s). SWAN divides this into 38 logarithmically distributed frequency bins with higher resolution for the lower frequencies.

The bathymetry is similar to the one from the Delft3D model, so based on the Aegean and Levantine dataset which is part of EMODNET bathymetry data.

Wind is the driving force for the waves and therefore an important input field for the model. The model is fed by spatial, time varying wind fields, similar to what is used in the Delft3D computations. For these preliminary runs, this data is produced by the NOAA GFS. The resolution of the wind fields is approximately 25 km and the time step is set at 6 hours.

Along the southern model boundary, a time and space varying wave boundary condition was imposed retrieving data from the MEDSEA WAM model (resolution  $1/24^\circ \times 1/24^\circ$ ) by ECMWF, available on Copernicus Marine Service (product MEDSEA-ANALYSIS-FORECAST-WAV-006-017). These data consist of hourly significant wave height, peak period and wave direction time-series. JONSWAP spectrum was chosen as the appropriate spectral shape and for the cosine power representing the directional spreading, a value of 2 was selected corresponding to  $31.5^\circ$  for the one-sided directional spread of the waves. Seven boundary locations have been specified along the southern side, between which SWAN interpolates the wave parameters.

longitude [°]	latitude [°]
24.512	40.269
24.753	40.269
24.990	40.271
25.223	40.269
25.463	40.267
25.709	40.268
25.945	40.269

Figure 4.2: longitude-latitude of the Swan grid

## 4.2 Results and Discussion

Using the above-described datasets provided by existing systems (GFS, TPXO, CMEMS), a series of preliminary runs of the hydrodynamic model was implemented to simulate on 5 days of hydrodynamic forecasts with a time step of 2 minutes. Model results were extracted every 60 mins.

### 4.2.1 Water Level

We study the water level, which is the elevation of the free water surface above some reference level, for five days from 16th of January 2019 to 21th of January 2019.

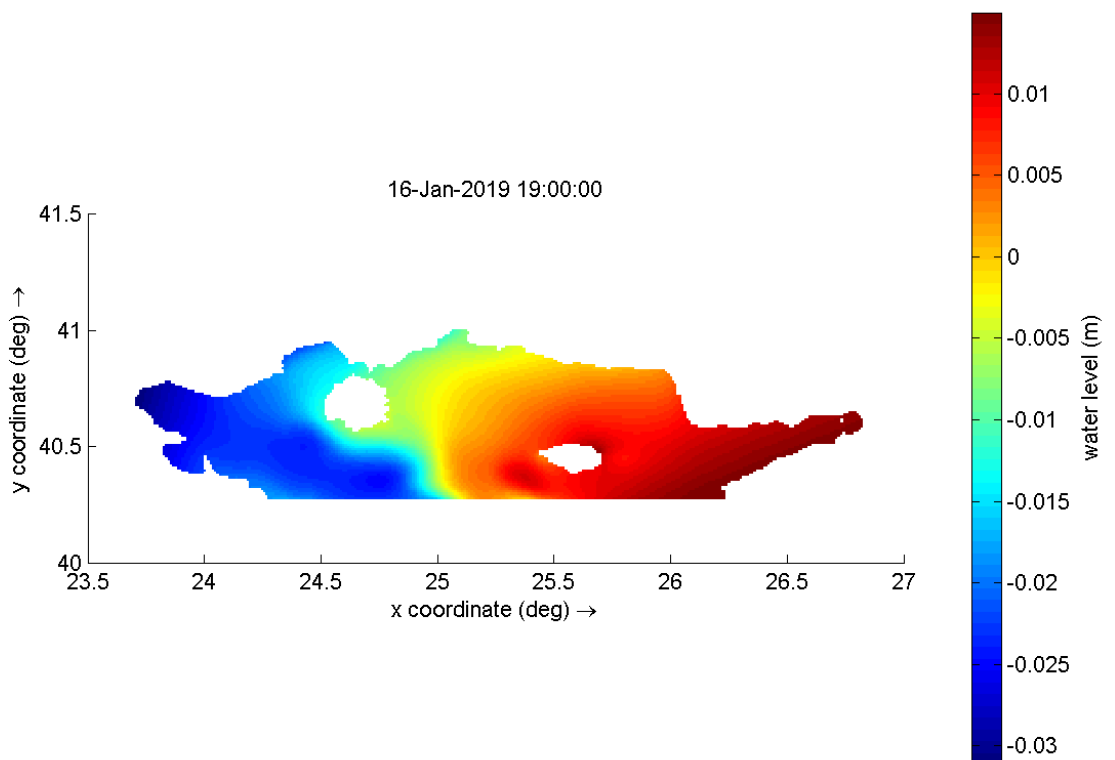


Figure 4.3: Water level - 16 January

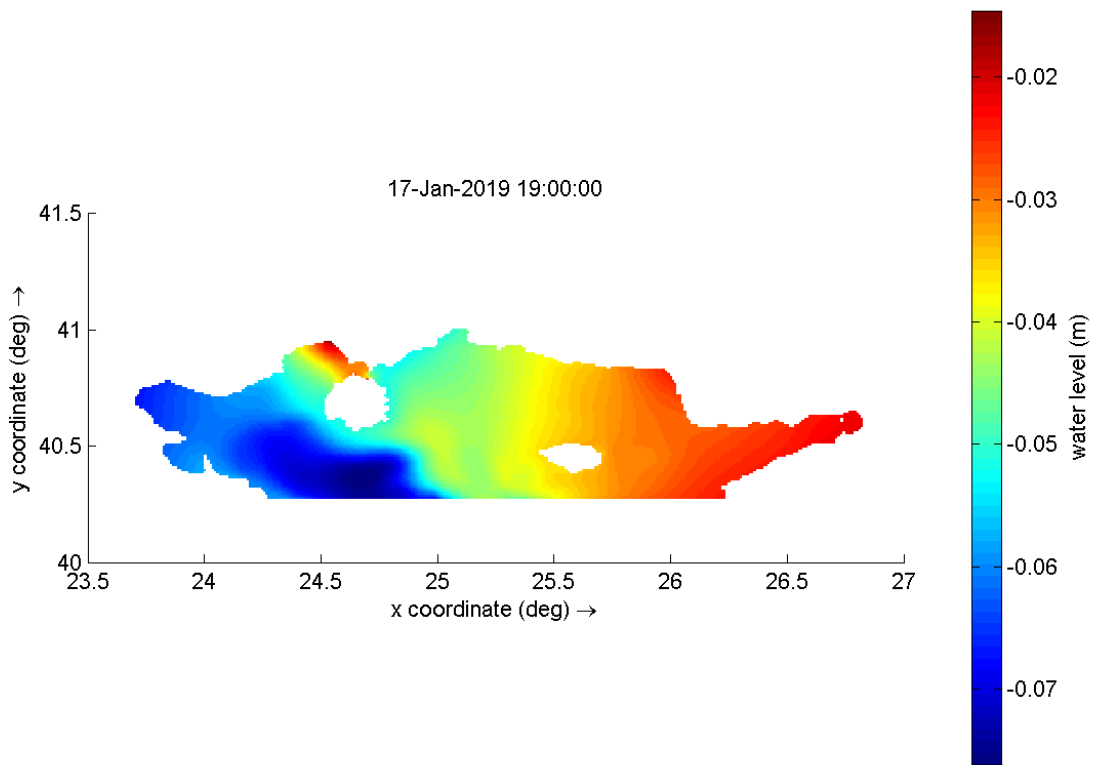


Figure 4.4: Water level - 17 January

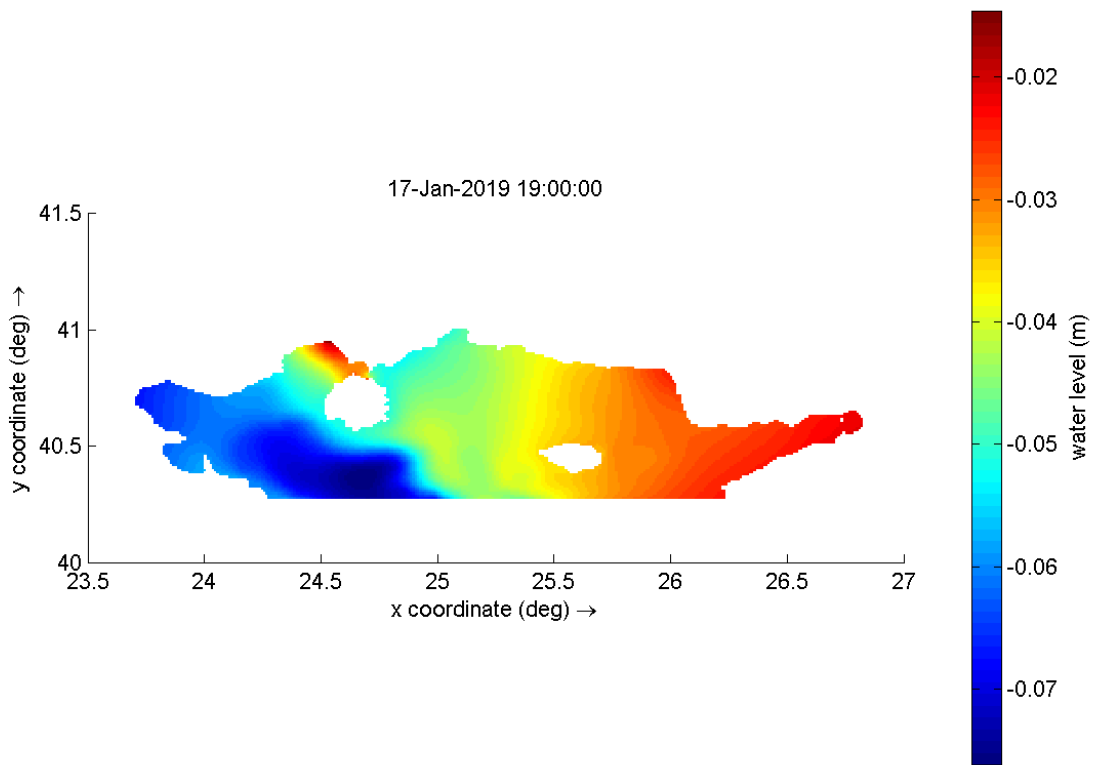


Figure 4.5: Water level - 17 January

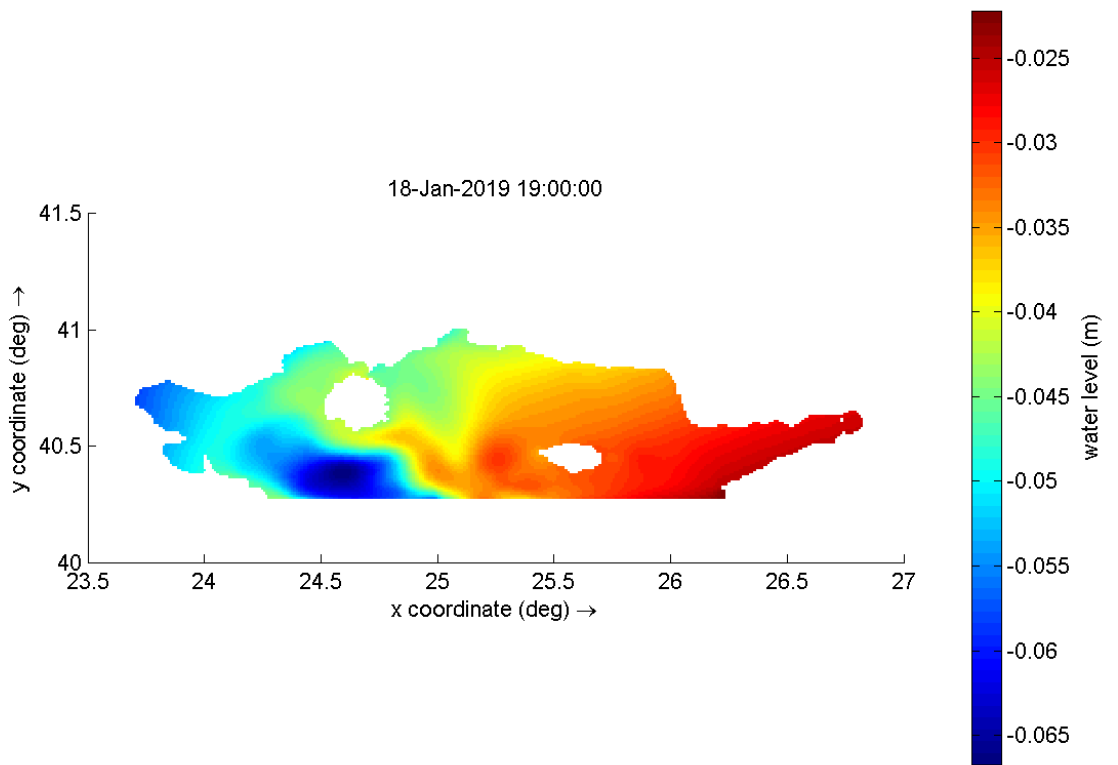


Figure 4.6: Water level - 18 January

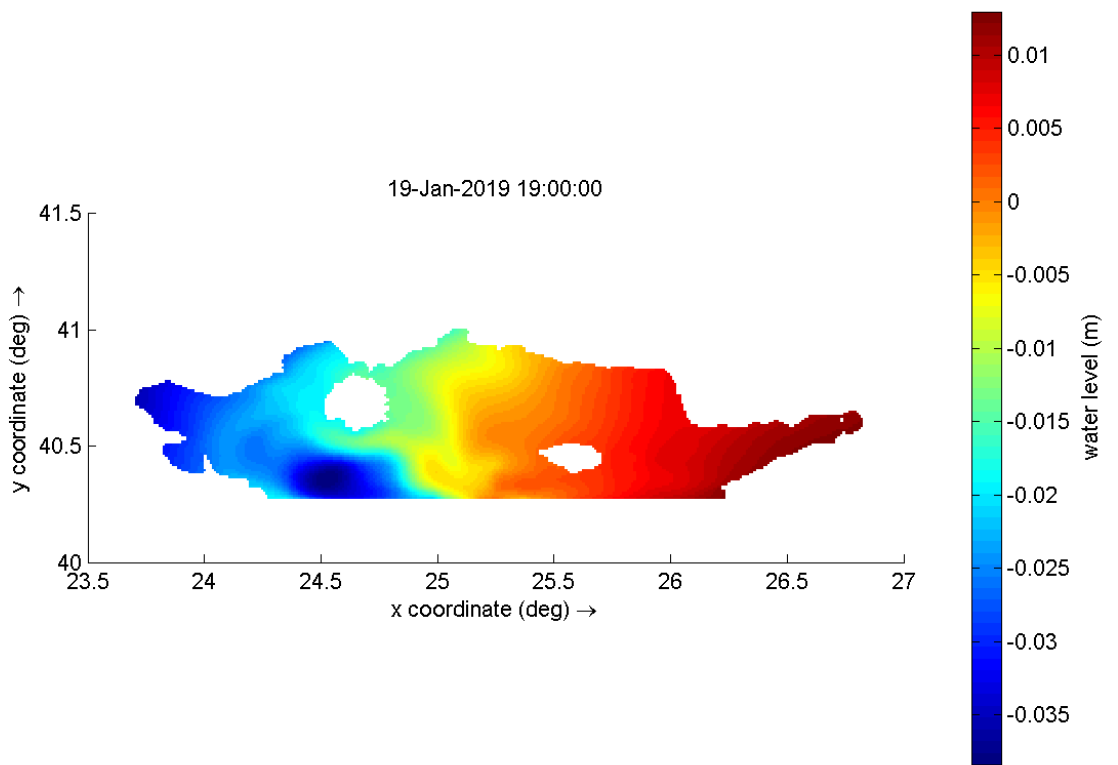


Figure 4.7: Water level - 19 January

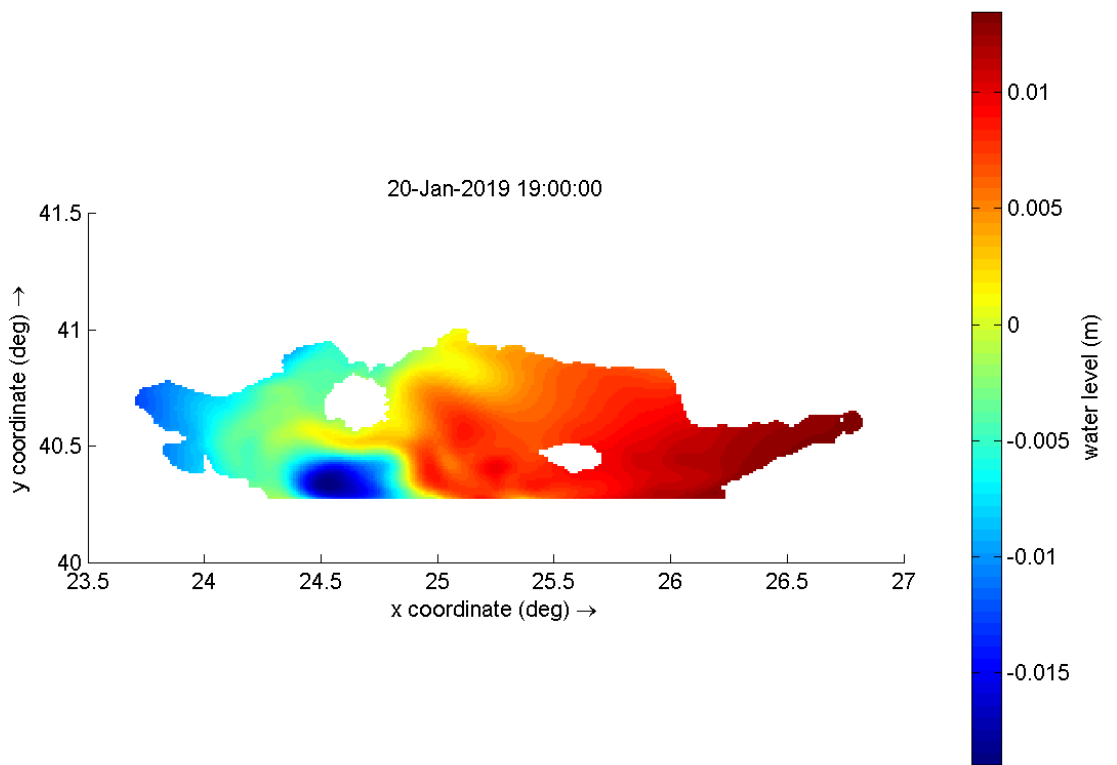


Figure 4.8: Water level - 20 January

We observe that the water level of our observation area is short in the whole period, near to 0m.

## 4.2.2 Currents

The following figures illustrate the current directions at selected times during the study period together with the associated current velocities through depth-averaged velocities and horizontal velocities. Depth-averaged velocity is the hydrodynamic speed, averaged over the depth. Currents ,in case of 2D computation are the speed and direction of the hydrodynamic depth-averaged flow. In case of 3D computation are the speed and direction of the hydrodynamic flow in a layer.

### Depth averaged velocity

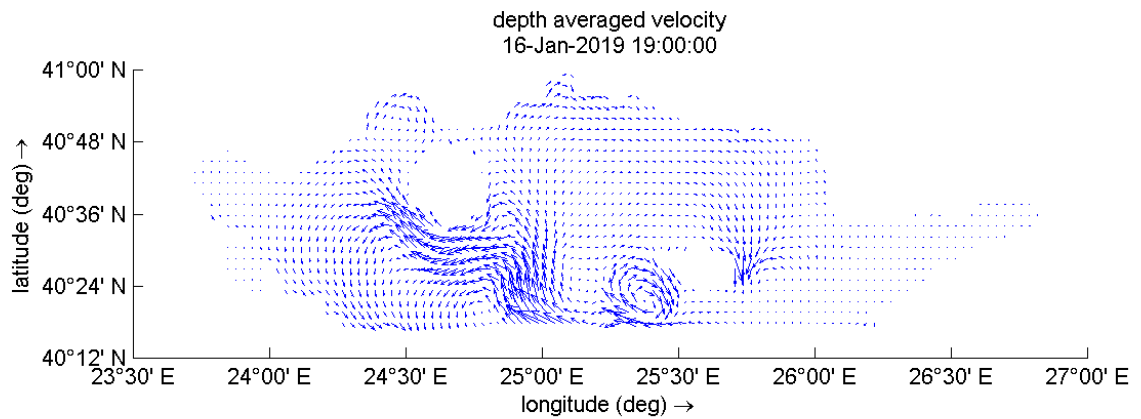


Figure 4.9: Depth averaged velocity -16 January

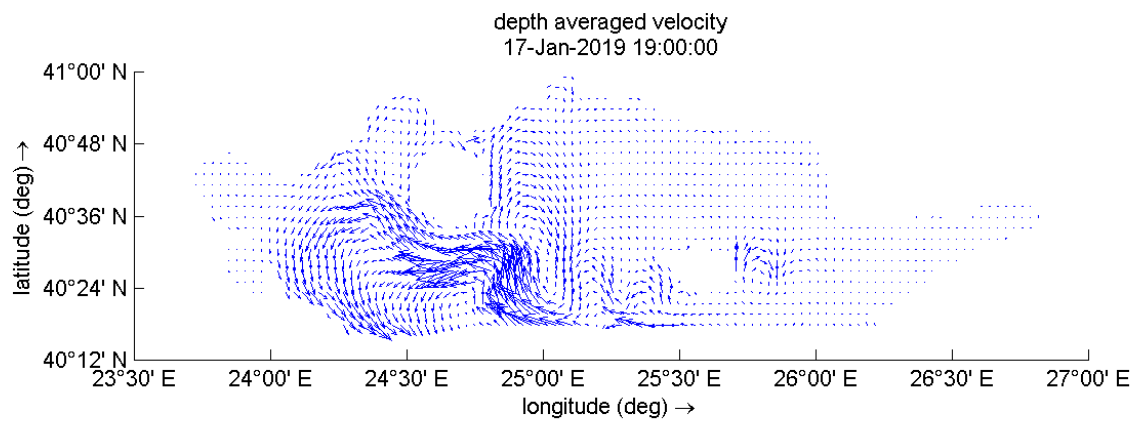


Figure 4.10: epth averaged velocity -17 January

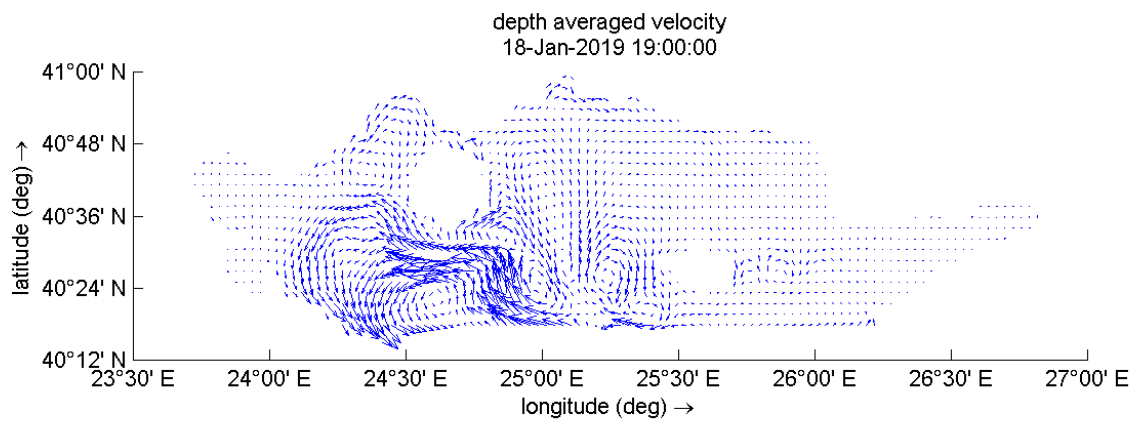


Figure 4.11: epth averaged velocity -18 January

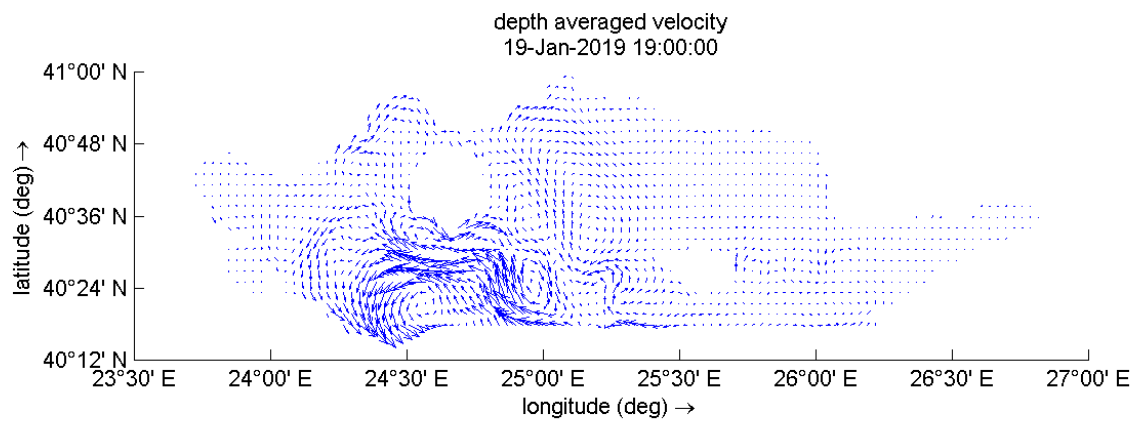


Figure 4.12: epth averaged velocity -19 January

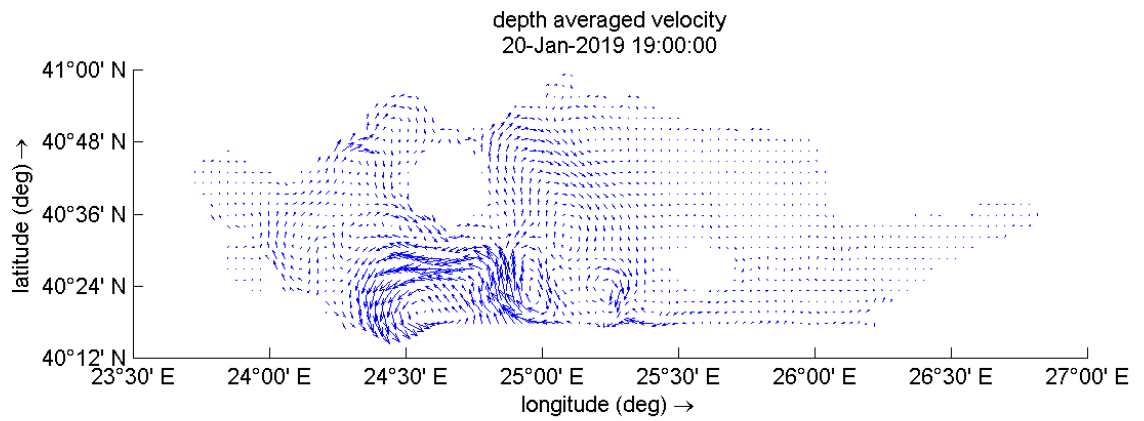


Figure 4.13: epth averaged velocity -20 January

We observe that the depth averaged velocity has generally low values in the Thracian Sea. In the East and North East Thracian Sea currents are negligible in the whole period of observation. We can see that the velocity is stronger South from the island Thassos and West and East of Samothraki island. More specifically, in the 18 and 19 January these currents are stronger than 17 and 20 January. These velocities depends on the wind speed and direction and on 3 discharges that we have in this area.

## Horizontal velocity

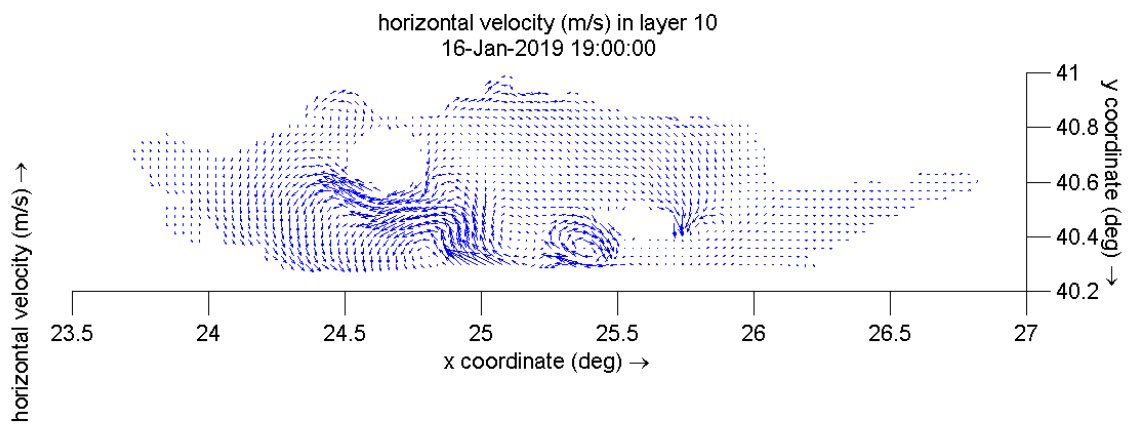


Figure 4.14: Horizontal velocity-16 January

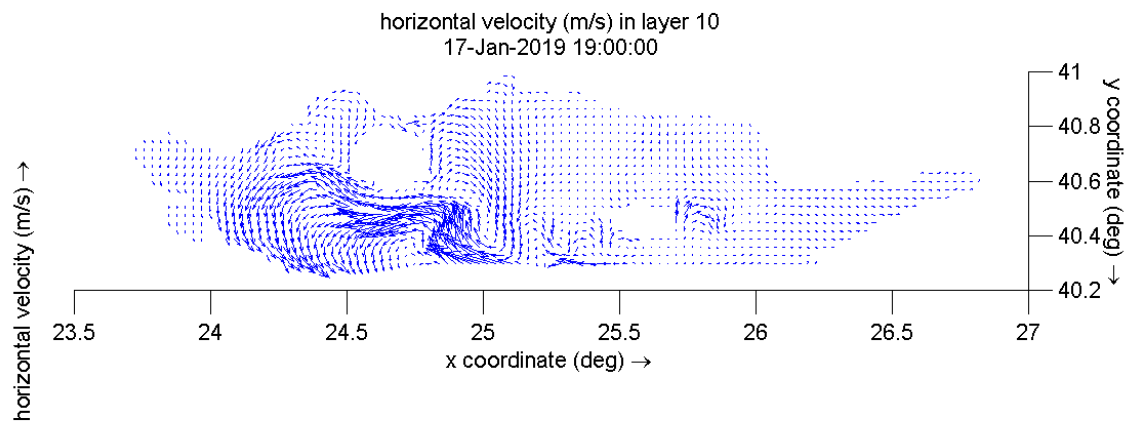


Figure 4.15: Horizontal velocity-17 January

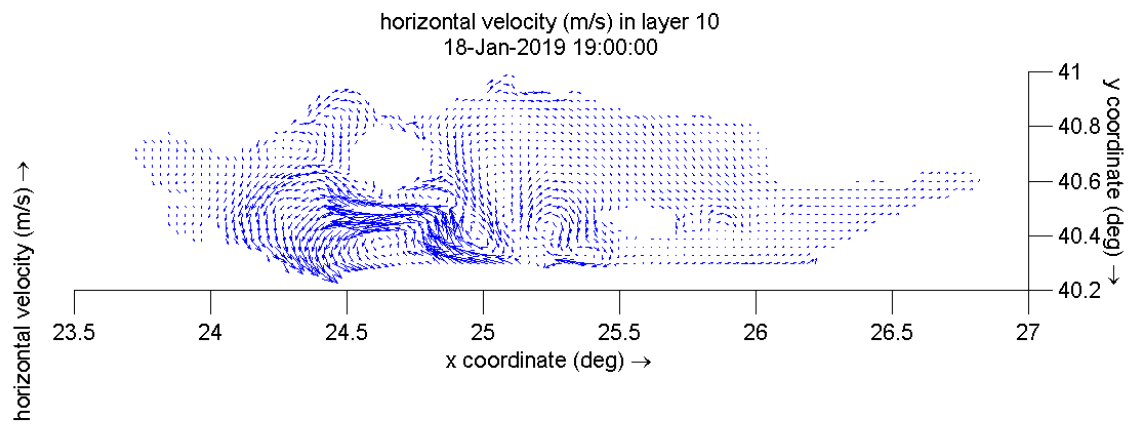


Figure 4.16: Horizontal velocity-18 January

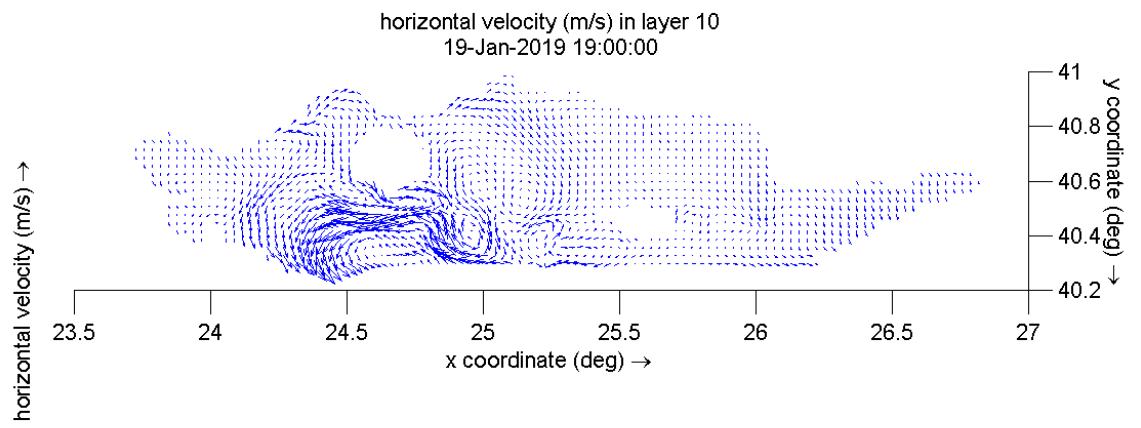


Figure 4.17: Horizontal velocity-19 January

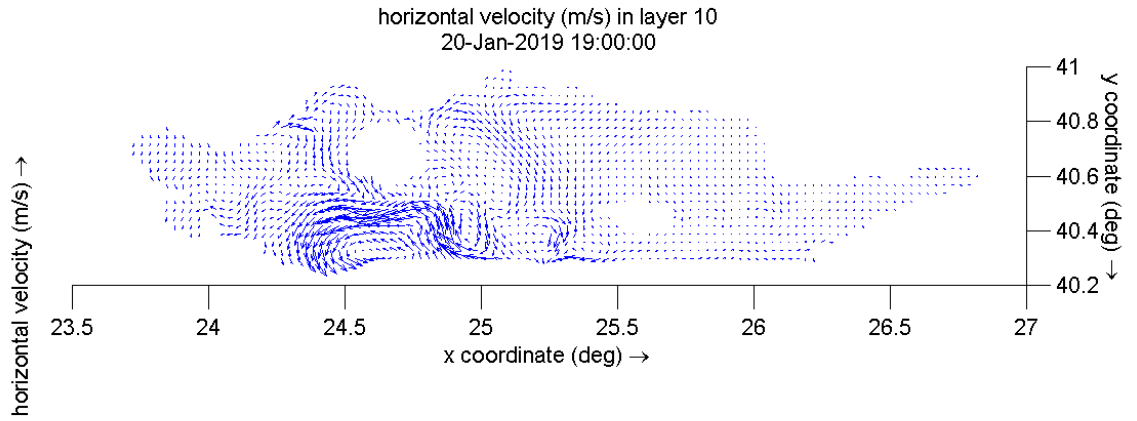


Figure 4.18: Horizontal velocity-20 January

We observe that the horizontal velocity has generally low values in the Thracian Sea. Especially, in the East and North East Thracian Sea currents are negligible in the whole period of observation. We can see that the horizontal velocity is stronger South from the island Thassos and West and East of Samothraki island. More specifically, in the 18 and 19 January there is an increase in the horizontal velocity and these values become smaller in the next days in 20 and 21 January. These velocities depends on the wind speed and direction and on 3 discharges that we have in this area.

### 4.2.3 Observation Points

We use two Observation stations, the Obs2 which is in the Kavala port and the Obs1 which is in the Kariani buoy. In fact they are monitoring points for current, water level and/or temperature and salinity. Moreover, observation points are defined at the centre of grid cells. Delft3D-FLOW writes the results of the simulation in this point to a history file which is a file that contains the results of a simulation in monitoring stations as a function of time. Thus, we study these two observation points through two different boundary conditions about the water level for 3 days, from 18-01-2019 to 21-01-2019 : the Water level for Riemann astronomic boundary and Riemann time series boundary. Finally, we make a comparison with the measurements of the Kavala station with the observation point Obs2 of our model in this period.

#### Riemann astronomic boundary for Water level

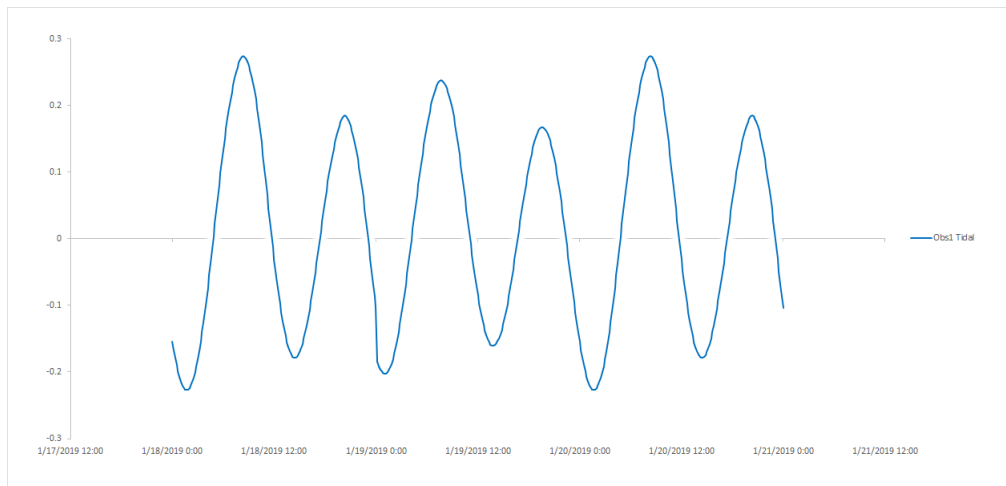


Figure 4.19: Obs1 Water level - Astronomic Boundary

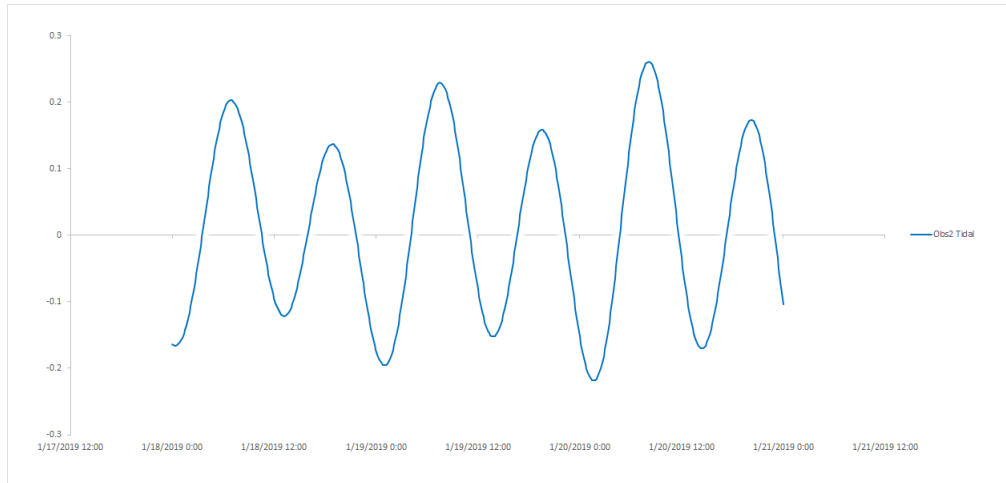


Figure 4.20: Obs2 Water level - Astronomic Boundary

We use the TXPO7.2 tidal solution to make the astronomic boundary conditions , which have semi-diurnal period, that is the phenomenon that is repeated every 12 hours. At the Obs1 observation point, the range of the water level is from -0.3m to 0.3 m. Furthermore, At the Obs2 observation point, the range of the water level is from -0.25 m to 0.2m .

## Comparison Obs2 with Kavala port station

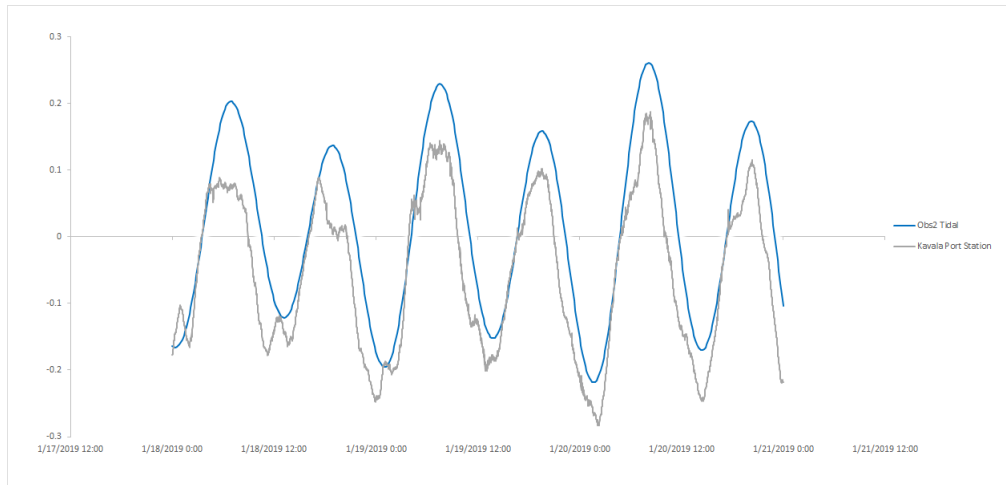


Figure 4.21: Comparison Obs2 with Kavala port station

We observe that the water level of these two different boundary conditions has the same phase of the oscillation. The measurements of the Kavala port station have both astronomic tidal and current time-series boundaries. Thus, there is that difference between these monitoring points.

## Riemann time-series boundary for Water level

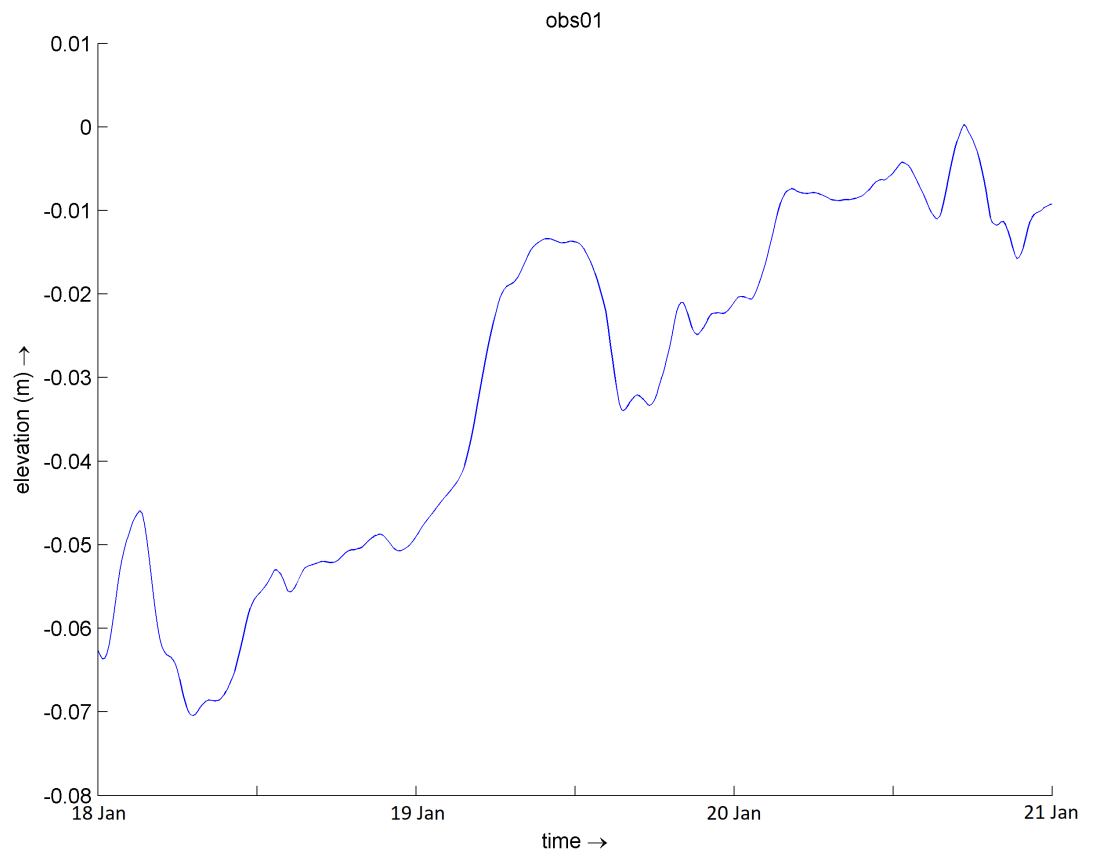


Figure 4.22: Obs1 Riemann Time-series

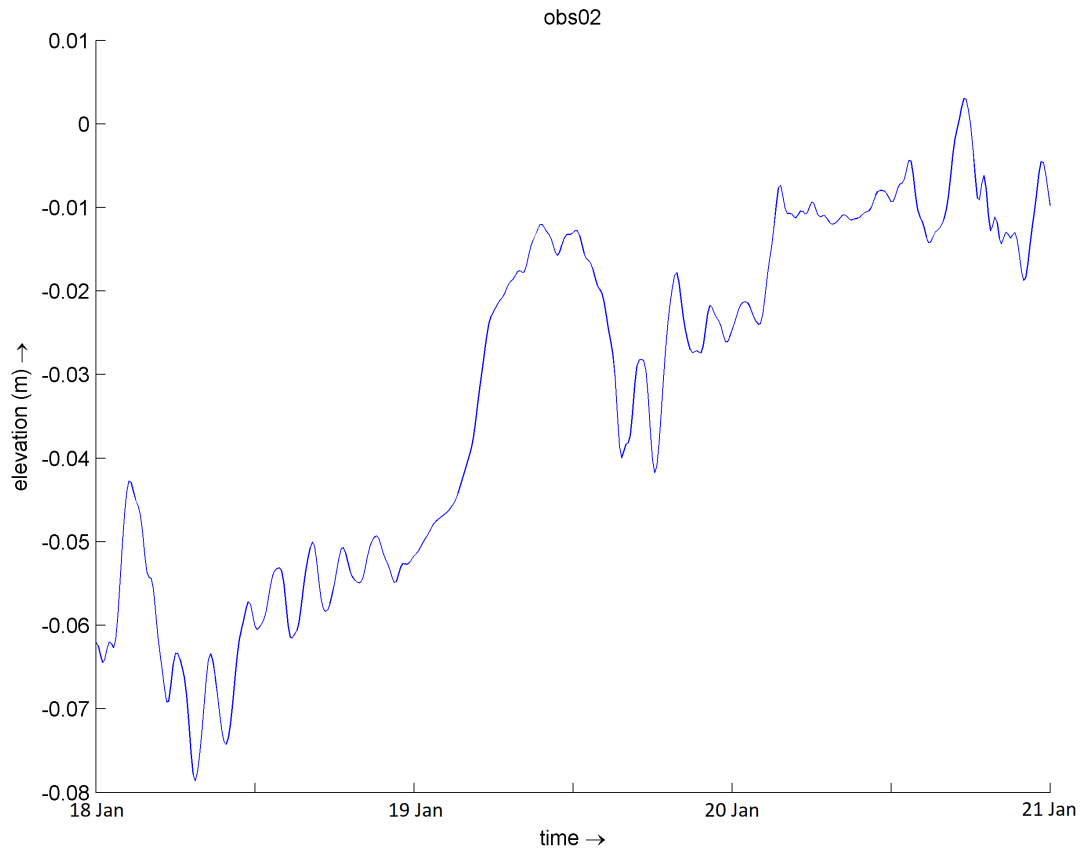


Figure 4.23: Obs2 Riemann time-series

We can see, that now without tidal, we have not a periodic motif. The water level has small values, near to 0m.

## 4.2.4 Swan Wave Model

The model provides various types of output. First of all, maps of wave parameters (significant wave height, wave direction, wave period, directional spreading) over the entire domain. Next, for a number of predefined locations, 1D and 2D wave spectra may be stored, as well as tables with various wave parameters. In the initial test the output format is ascii (tables of wave spectra) and matlab mat les (maps).

The period January 16, 2019 to January 21, 2019 was selected for initial tests. Wind and wave les were downloaded and adjusted to the proper input format for SWAN. In Figure 30 the boundary signals for this test period are shown. The upper panel shows the series of the significant wave height,  $H_{m0}$  [m], this value will be prescribed on all specified wave boundaries. The second panel the peak period,  $T_p$  [s], the peak period is defined as the wave period associated with the most energetic waves in the total wave spectrum at a specific point. The latest panel is the direction of the waves  $Dir$  [°]. The directional is given by the direction where the waves come from. This period is used as initial test, since it consists of both large and small wave heights from different directions.

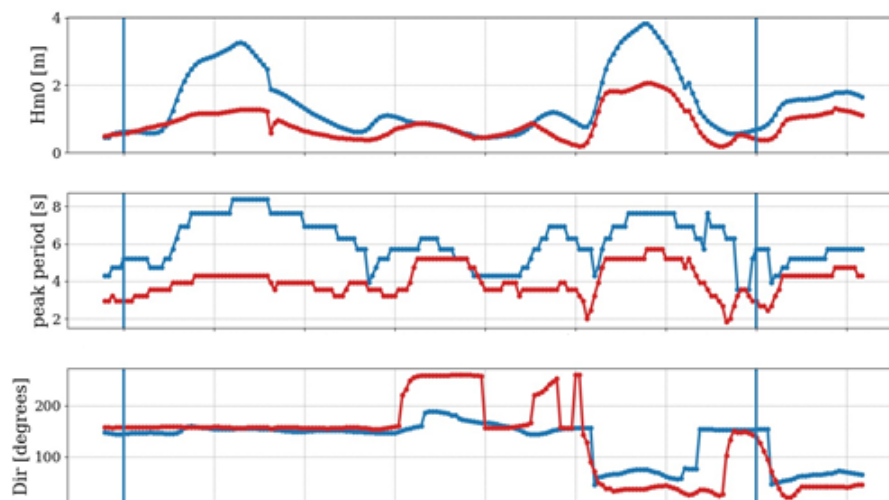


Figure 4.24: Boundary Conditions of the modeled period. The blue line represents the most Westward boundary point (Blue dot in figure 30) and the red line represent the most Eastward point of the boundary.

We observe that the significant wave height ( $H_{m0}$ ) at the Westward boundary point (blue line) reaches a maximum value of 4m, on 19th with 20th of January, whereas the Eastward point of boundary (red line) reaches a maximum value of 2m. Generally, almost in the whole time of period the significant wave height ( $H_{m0}$ ) at the Westward boundary point is higher from the Eastward point of boundary.

In the operational environment we suggest starting each run with an initial wave field resulting from a previous run (a so called 'hot-start') and to apply a 48 hr forecast horizon.

Preliminary results are given in the following plots. The computational time is in the order of 45 min for a 48 hr forecast.

Now we select the day of 18th January of 2019 to observe the significant wave height  $H_{m0}$  and the mean absolute wave period (in s),  $T_{mm10}$ . Moreover we select 6 points to compare their significant wave heights.

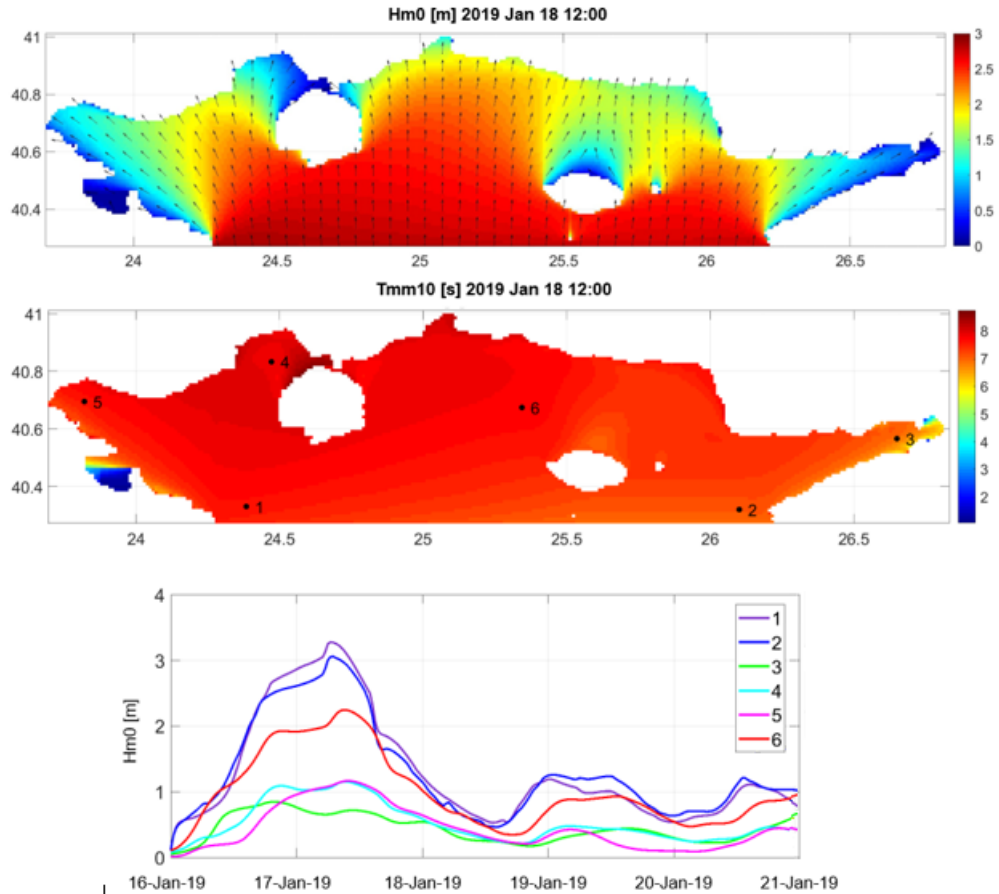


Figure 4.25: Preliminary Results of SWAN Thracian Model

We observe that the range of the significant wave height  $H_{m0}$  is from 0m to 3m. The higher height is observed at the South boundaries of Thracian Sea and the shorter height near to the coastal zone, something that we expected. On the otherwise, the mean absolute wave period (in s),  $T_{mm10}$  is bigger near to kalava port and the island Thassos, that is the Northwest of the Thracian Sea. Finally, in the third graphic we can see that the largest significant wave height  $H_{m0}$  are at the points 1 and 2 which are near to the South boundaries. Specifically, the highest height is on 17th with 18th January 2019 at these points with value 3m and the lowest on the 18th with 19th January. At the point 6 that is near to the center of

our observation area, the maximum value is 2m on the 16th with 17th January of 2019. At the points 1,2,3 which are near to the coastal zone is observed that they have smaller significant wave heights with maximum value 1m on the 16th with 17th January of 2019.

#### **4.2.5 Conclusion and Recommendations**

The results of the simulation give very satisfactory characteristics concerning the overall view of the study area. A Flow and SWAN model has been set up for the Thracian Sea Observatory, based on the grid of the Delft3D hydrodynamic model. The preliminary results make sense, but calibration and validation are recommended. For a proper calibration, wave observations are necessary. Attention must be paid to spatial resolution, boundary conditions (including its locations), directional spreading, wind drag formulation, time step, convergence, lead time and required output (locations, parameters and format). These can be relatively easily changed once suitable values are known. If reliable outputs near the shoreline have been provided, a higher spatial resolution is required to better include the gradients in bathymetry.

# Chapter 5

## References

# Bibliography

- [1] Deltares, Delft3D - FLOW. Simulation of multi-dimensional hydrodynamic flows and transport phenomena, including sediments. Delft., 2013
- [2] Deltares, Delft3D - WAVE. Simulation of short-crested waves with SWAN. Delft, 2013
- [3] ISMAR-CNR, SHYFEM. Finite Element Model for Coastal Seas, User's Manual. 2014
- [4] Deltares Swan team, Swan scientific and technical documentation. Delft University of Technology, Delft, Netherlands. 1993-2019
- [5] Grant, W. D. and O. S. Madsen, Combined wave and current interaction with a rough bottom. *Journal of Geophysical Research* 84 (C1): 17971808. 1979
- [6] Holthuijsen, L.H., *Waves in oceanic and coastal waters*. Cambridge University Press, New York, USA. 2007
- [7] Jin X.Y., Quasi-three-dimensional numerical modelling of flow and dispersion in shallow water. Ph.D. thesis, Delft University of Technology, 1993.
- [8] Stelling G. S., On the construction of computational methods for shallow water flow problems. Tech. Rep. 35, Rijkswaterstaat. 1984
- [9] Stelling, G. S. and J. A. T. M. van Kester. 1994. On the approximation of horizontal gradients in sigma co-ordinates for bathymetry with steep bottom slopes. *International Journal Numerical Methods In Fluids* 18: 915955.
- [10] Stelling, G. S. and J. J. Leendertse, 1992. Approximation of Convective Processes by Cyclic AOI methods. In M. L. Spaulding, K. Bedford and A. Blumberg, eds., *Estuarine and coastal modeling, Proceedings 2nd Conference on Estuarine and Coastal Modelling*, ASCE, 771-782 pp
- [11] Whitham, G., *Linear and nonlinear waves*. Wiley, New York. 1974
- [12] Egbert, Gary D. and Erofeeva, Svetlana Y. Efficient inverse modeling of barotropic ocean tides. 2002. *Journal of Atmospheric and Oceanic Technology*, 183-204. doi:10.1175/1520-0426(2002)019

- [13] Hasselmann, K., T. P. Barnett, E. Bouws, H. Carlson, D. E. Cartwright, K. Enke, J. Ewing, H. Gienapp, D. E. Hasselmann, P. Kruseman, A. Meerburg, P. Miller, D. J. Olbers, K. Richter, W. Sell and H. Walden, Measurements of wind wave growth and swell decay during the Joint North Sea Wave Project (JONSWAP). *Deutsche Hydrographische Zeitschrift* 8 (12).1973
- [14] Panton, I. Ronald. 2013. *Incompressible Flow*. John Wiley & Sons, 4 edition, 913 pp.
- [15] Reynolds O., On the dynamical theory of incompressible viscous fluids and the determination of the criterion. *Philosophical transactions of the royal society*, 186, 1894
- [16] Ris, R. C., *Spectral Modelling of Wind Waves in Coastal Areas*. Communications on Hydraulic and Geotechnical Engineering, report 97-4. Delft University of Technology, Delft, The Netherlands. Ph.D. thesis. 1997
- [17] Komen, G. J., Cavaleri, L., Donelan, M., Hasselmann, S., K., Hasselmann, S., Janssen P. A. E. M. 1994. *Dynamics and Modelling of Ocean Waves*. Cambridge University Press, 532 pp.
- [18] Dean, Robert G., Dalrymple, Robert A. 2001. *Coastal Process with engineering applications*. Cambridge University Press, 475 pp.
- [19] Dean, Robert G., Dalrymple, Robert A. 1991. *Water Wave Mechanics for Engineers and Scientists*. Cambridge University Press, 368 pp.
- [20] Givoli, D. 1992. *Numerical methods for problems in infinite domains*. Elsevier Science 316 pp.
- [21] Lesser, G. R., Roelvink, J. A., Van Kester, J. A. T. M., Stelling, G. S., 2004. Development and validation of a three-dimensional morphological model. *Coastal Engineering* 51: 883-915 pp.
- [22] MIKE21 & MIKE3 flow model FM, hydrodynamic module, Short description, DHI, 23-06-2011.
- [23] MIKE21 wave modeling, MIKE21 SW spectral waves FM, Short description, DHI, 23-06-2011.
- [24] Young, I. R. 1999. *Wind Generated Ocean Waves*, Elsevier, 287 pp.
- [25] Roelvink, J. A. and D. J. R. Walstra, Keeping it simple by using complex models. In *Proceedings of the 6th International Conference on Hydro-Science and Engineering*. Advances in Hydro-Science and Engineering, vol. VI, page p. 12. Brisbane, Australia. 2004
- [26] The Wamdi Group. 1988. *The WAM Model A Third Generation Ocean Wave Prediction Model*. *Journal of physical oceanography*, 18, 1810. doi:10.1175/1520-0485(1988)018

- [27] Verboom, G. K. and A. Segal, 1986. Weakly reflective boundary conditions for shallow water equations. In 25th Meeting Dutch Working group on Numerical Flow Simulations, Delft. Delft University of Technology, Delft, The Netherlands.
- [28] Verboom, G. K. and A. Slob, 1984. Weakly-reflective boundary conditions for two-dimensional water flow problems. *Advances in water resources* 7 (4): 192-197.